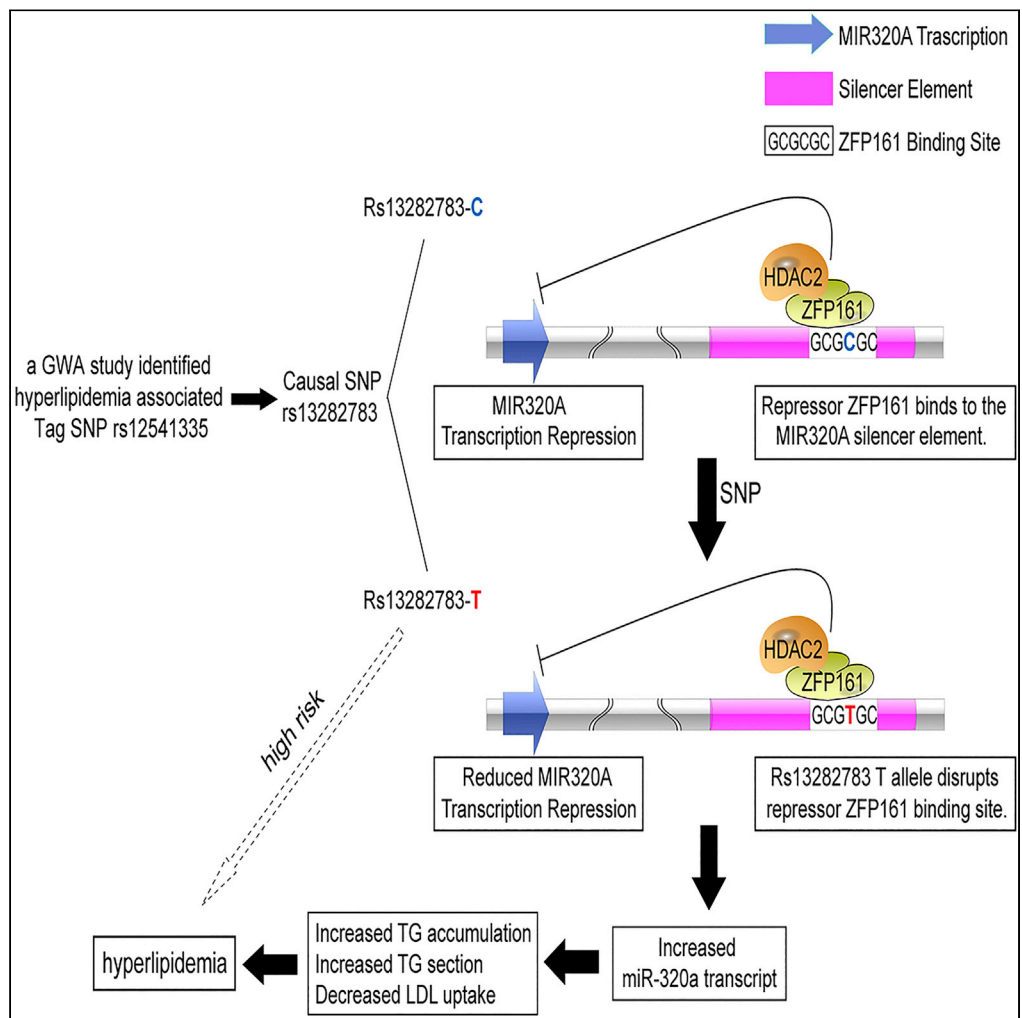


Article

A Key GWAS-Identified Genetic Variant Contributes to Hyperlipidemia by Upregulating miR-320a



Zhongwei Yin,
Yanru Zhao,
Hengzhi Du, ...,
Zheng Wen, Chen
Chen, Dao Wen
Wang

chenchen@tjh.tjmu.edu.cn
(C.C.)
dwwang@tjh.tjmu.edu.cn
(D.W.W.)

HIGHLIGHTS

Hepatic miR-320a overexpression led to hyperlipidemia, not vice versa

A hyperlipidemia-associated SNP rs13282783 distally regulated miR-320a expression

miR-320a promoted TG accumulation and repressed LDL-C uptake in hepatocytes



Article

A Key GWAS-Identified Genetic Variant Contributes to Hyperlipidemia by Upregulating miR-320a

Zhongwei Yin,^{1,2} Yanru Zhao,^{1,2} Hengzhi Du,^{1,2} Xiang Nie,¹ Huaping Li,¹ Jiahui Fan,¹ Mengying He,¹ Beibei Dai,¹ Xudong Zhang,¹ Shuai Yuan,¹ Zheng Wen,¹ Chen Chen,^{1,3,*} and Dao Wen Wang^{1,*}

SUMMARY

It has been unclear whether the elevated levels of the circulating miR-320a in patients with coronary artery disease is due to environmental influence or genetic basis. By recombinant adeno-associated virus (rAAV)-mediated loss- and gain-of-function studies in the mouse liver, we revealed that elevated miR-320a is sufficient to aggravate diet-induced hyperlipidemia and hepatic steatosis. Then, we analyzed the data from published genome-wide association studies and identified the rs12541335 associated with hyperlipidemia. We demonstrated that the rs13282783 T allele indeed obligated the silencer activity by preventing the repressor ZFP161 and co-repressor HDAC2 from binding to DNA that led to miR-320a upregulation. We further confirmed this genetic connection on an independent population and through direct genome editing in liver cells. Besides environmental (diet) influence, we established a genetic component in the regulation of miR-320a expression, which suggest a potential therapeutic avenue to treat coronary artery disease by blocking miR-320a in patient liver.

INTRODUCTION

Hyperlipidemia is the most common risk factor for coronary artery disease (CAD) (Benjamin et al., 2019; Go et al., 2013; Yusuf et al., 2004). Despite progress in the treatment of elevated plasma triglyceride (TG) and cholesterol levels using fibrates and statins, CAD remains the leading cause of human morbidity and mortality worldwide (Benjamin et al., 2019). Further understanding of regulators that control lipid homeostasis may facilitate the design of new therapeutic strategies and drugs for hyperlipidemia and CAD.

MicroRNAs (miRNAs) are the most studied class of noncoding RNAs. Typically serving as post-transcriptional regulators of mRNA (Hammond, 2015), miRNAs are crucial mediators in multiple biological processes, including lipid metabolism (Rayner et al., 2010; Sadiq et al., 2017). Accumulating evidence suggests that aberrantly expressed miRNAs lead to various diseases (Hanin et al., 2018; Zhao et al., 2017), underscoring the importance of elucidating molecular mechanisms that regulate the expression of miRNAs.

Genome-wide association studies (GWASs) are extensively used to identify genetic variants associated with common traits, including diseases (Consortium et al., 2013; Sabatti et al., 2009; Willer et al., 2013). Characterizing variants can provide opportunities for the discovery of new biological processes and therapeutic targets for corresponding conditions (Atanasovska et al., 2015; Cohen, 2016; Teslovich et al., 2010; Turcot et al., 2018). Although variants in coding regions are more readily interpreted as influential on protein function and stability, most GWAS-identified variants lie in non-coding regions (Freedman et al., 2011; Maurano et al., 2012). Functional characterization of these loci is currently the greatest challenge in the post-GWAS era (Freedman et al., 2011; Maurano et al., 2012; Visscher et al., 2017). Recent studies suggested that these non-coding variants are enriched in putative distal transcriptional regulatory elements, including enhancers, silencers, and insulators (Du et al., 2015; Maurano et al., 2012; Zhang et al., 2014). Such variants appear to influence remote target-gene expression through modulating transcription factors (TFs) that bind to regulatory elements in disease-specific cell types (Hayashi et al., 2016; Painter et al., 2016; Ye et al., 2016). Studies aiming to understand the functional consequences of variants on long-range regulatory elements have mainly investigated protein-coding gene regulation. However, potential effects on miRNA expression remain largely unexplored.

¹Division of Cardiology, Department of Internal Medicine and Hubei Key Laboratory of Genetics and Molecular Mechanisms of Cardiological Disorders, Tongji Hospital, Tongji Medical College, Huazhong University of Science and Technology, Wuhan 430030, China

²These authors contributed equally

³Lead Contact

*Correspondence: chenchen@tjh.tjmu.edu.cn (C.C.), dwwang@tjh.tjmu.edu.cn (D.W.W.)

<https://doi.org/10.1016/j.isci.2020.101788>



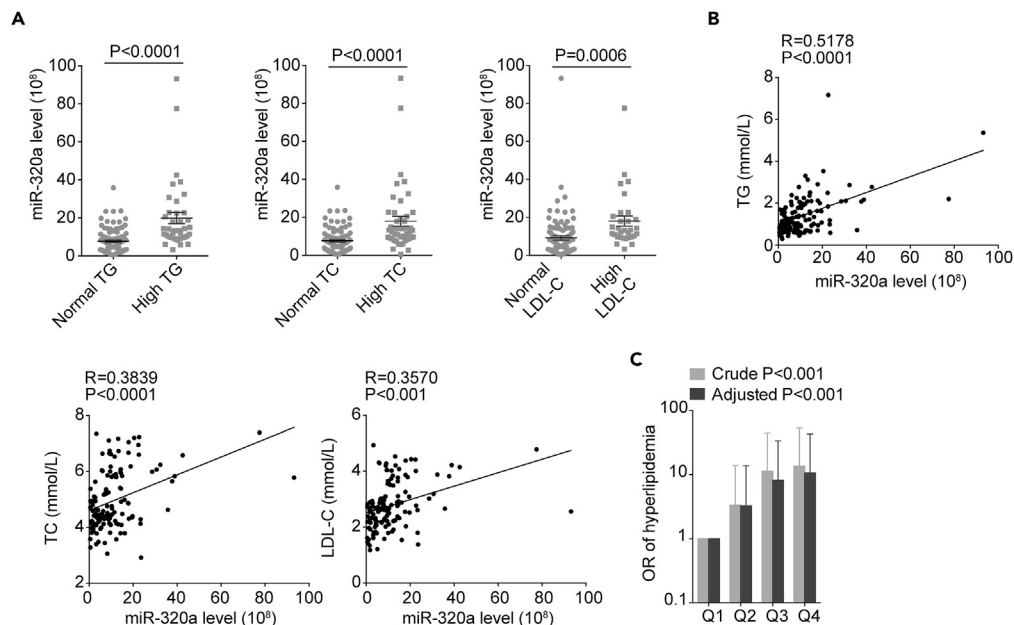


Figure 1. Circulating miR-320a Level was Elevated in Men with Hyperlipidemia

(A) The levels of circulating miR-320a in men with normal and high TG, normal and high TC, as well as normal and high LDL-C (n = 91 for normal TG; n = 39 for high TG; n = 84 for normal TC; n = 46 for high TC; n = 99 for normal LDL-C; n = 31 for high LDL-C. Data are expressed as mean \pm SEM, Student's t test).

(B) The correlation of circulating miR-320a levels with TG, TC, or LDL-C in men (n = 130, the p values were produced by Pearson correlation analysis).

(C) ORs (crude or adjusted for BMI) of hyperlipidemia stratified by quartile level of circulating miR-320a (n = 130). Logistic regression with and without adjustment for BMI was used, and data are expressed as ORs and their 95% CIs). Q1, first quartile; Q2, second quartile; Q3, third quartile; Q4, fourth quartile; TG, triglyceride; TC, total cholesterol; LDL-C, low-density lipoprotein cholesterol; CI, confidence interval; OR, odds ratio.

See also [Figures S1](#) and [S2](#), and [Tables S1–S3](#), and [S12](#).

We previously reported that miR-320a contributed to CAD through augmenting multiple risk factors and impairing endothelial cell function ([Chen et al., 2015](#)). We also noticed that miR-320a is differentially expressed in livers of C57Bl/6J mice and ApoE^{-/-} mice, associated with their distinct plasma lipid profiles ([Chen et al., 2015](#)). Previous research has identified the promoter sequence of miR-320a and noted its unusual biogenesis ([Xie et al., 2013](#)). Pre-miR-320a is an RNA Pol II transcript, with the 5'- and 3'-ends directly generated via transcription initiation and termination ([Xie et al., 2013](#)). After Dicer processing, only 3p-miRNA is efficiently loaded onto the Argonaute complex, while 5p-miRNA degrades ([Xie et al., 2013](#)). Therefore, MIR320A gene only generates a single 3p-miRNA, called miR-320a.

Here, we investigated the role and regulation of miR-320a in hyperlipidemia. We showed that hepatic miR-320a is crucial for the development of diet-induced hyperlipidemia and fatty liver. Overexpressing miR-320a aggravated TG accumulation and secretion and reduced low-density lipoprotein (LDL) uptake in liver cells. High-fat treatment *in vivo* and *in vitro* did not change miR-320a expression. Therefore, we hypothesized that a genetic mechanism is responsible for miR-320a dysregulation in hyperlipidemia. Through re-analyzing available GWAS data and the following functional studies, we identified a potential mechanism involving a hyperlipidemia-associated variant within a silencer region. This risk allele of variant led to miR-320a dysregulation via influencing ZFP161 and HDAC2 binding efficiency.

RESULTS

Circulating miR-320a Was Significantly Elevated in Patients with Hyperlipidemia

We found that plasma miR-320a levels were significantly elevated in individuals with high TG, total cholesterol (TC), and low-density lipoprotein cholesterol (LDL-C) ([Figures 1A](#) and [S1A–S1C](#)). Additionally, we found that the plasma miR-320a was positively correlated with TG, TC, and LDL-C levels, a pattern that

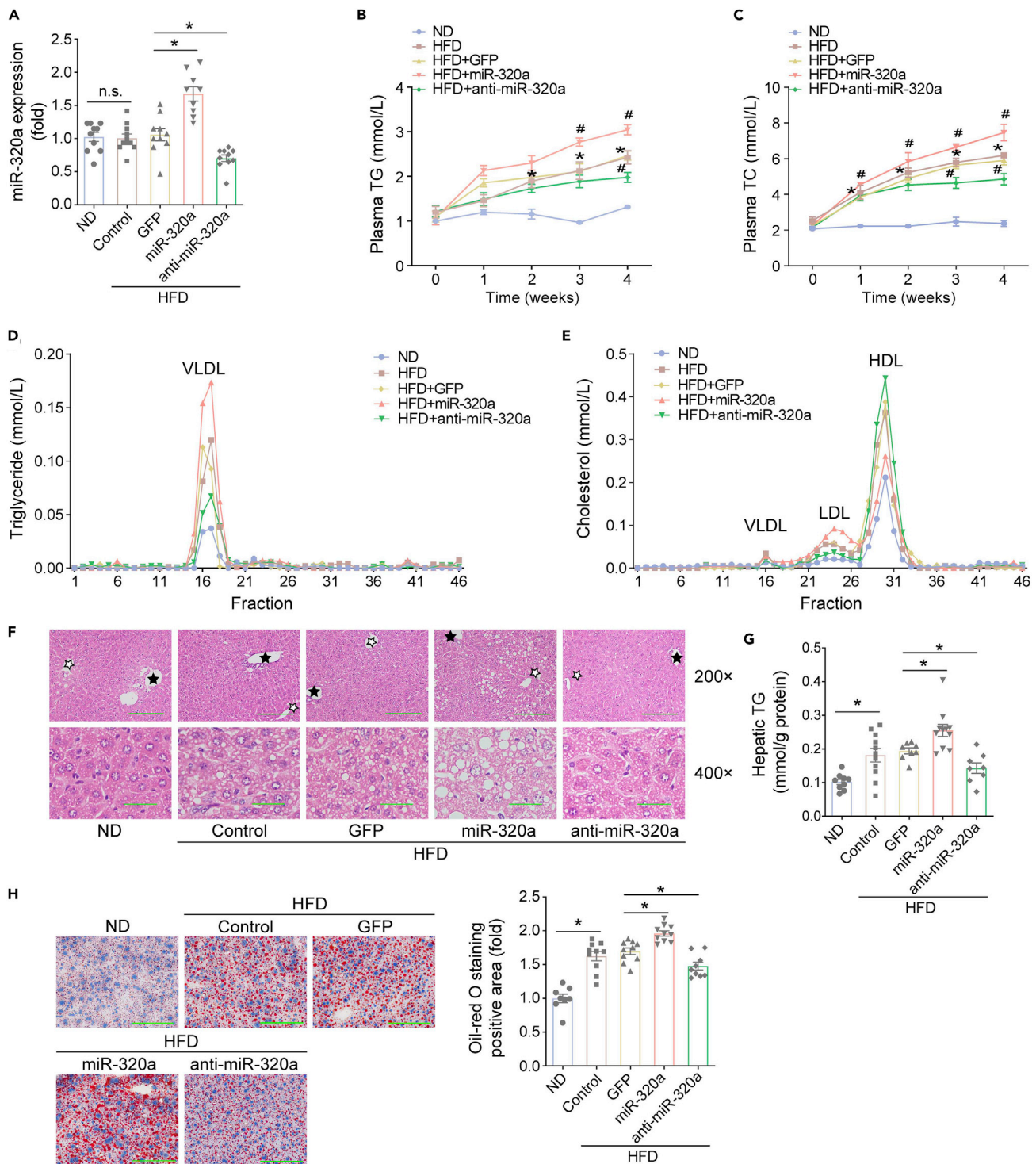


Figure 2. Liver-Specific miR-320a Overexpression Aggravated Diet-Induced Hyperlipidemia and Hepatic Steatosis in Mice

C57BL/6J mice were first injected with the corresponding rAAVs or normal saline in the caudal vein at 6 weeks of age. After 2 weeks, infected mice were subjected to normal diet or high-fat diet, respectively, for 4 weeks.

(A) miR-320a expression was determined by real-time PCR in the liver tissues of mice (n = 9–11).

(B and C) Development of TG (B) and TC (C) levels in the plasma of mice (n = 5–7 per group at indicated time points). Data are expressed as mean \pm SEM; *p < 0.05 vs. ND group; #p < 0.05 vs. HFD + GFP group, Student's t test.

(D and E) Triglyceride (D) or cholesterol (E) content of FPLC-fractionated lipoproteins of pooled plasma from each group (n = 9–11 per group).

Figure 2. Continued

(F) TG content in liver tissues of mice (n = 9–11).

(G) Representative images of hematoxylin and eosin (H&E) staining of liver sections. Scale bar represents 100 μ m for 200 \times and 25 μ m for 400 \times . The solid star indicates the central vein; the hollow star indicates the portal tract.

(H) Representative images and quantitative analysis of oil red O staining of lipid deposition in liver sections (n = 8–10 mice per group). Scale bar represents 100 μ m. For (A), (G), and (H), data are expressed as mean \pm SEM, *p < 0.05, Student's t test. ND, normal diet; HFD, high-fat diet; VLDL, very low-density lipoprotein; HDL, high-density lipoprotein.

See also Figure S3.

was more pronounced in men (Figures 1B and S2A–S2C). Circulating miR-320a was significantly correlated with several other metabolic parameters, including body mass index (BMI), blood glucose level, and blood pressure (Tables S1–S3). Because obesity is a risk factor for diabetes mellitus and hyperlipidemia (Wahl et al., 2017), we performed partial correlation analysis for miR-320a and metabolic variables. After adjustments for BMI and age, circulating miR-320a remained significantly correlated with TG, TC, and LDL-C but not with other metabolic parameters. This outcome suggests that miR-320a has an independent effect on blood lipid modulation (Tables S1–S3). Moreover, BMI-adjusted odds of hyperlipidemia progressively increased from the first to the fourth quartile of miR-320a level in both sexes (Figures 1C, S1C, and S2C). In men, the odds ratio of hyperlipidemia was 3.26 (95% confidence interval [CI]: 0.77–13.81) for the second quartile relative to the first, 8.14 (95% CI: 1.96–33.81) for the third quartile, and 10.59 (95% CI: 2.588–43.287) for the fourth quartile (Figure 1C).

Liver-Specific miR-320a Overexpression Aggravated Diet-Induced Hyperlipidemia and Hepatic Steatosis in Mice

Based on the results just described and the importance of the liver to lipid metabolism, we investigated the effects of hepatic miR-320a on blood lipids in high-fat diet (HFD)-fed mice. Immunohistochemical staining showed that green fluorescent protein (GFP) was specifically expressed in the liver of rAAV-TBG-GFP-treated mice (Figure S3A), demonstrating the tissue-specificity of the rAAV-mediated manipulations. As expected, rAAV-TBG-miR-320a treatment increased miR-320a expression, while rAAV-TBG-anti-miR-320a decreased expression (Figure 2A). Weekly blood sampling tests revealed that plasma TG and TC levels of HFD mice progressively increased compared with normal-diet (ND)-fed mice (Figures 2B and 2C). Moreover, miR-320a overexpression significantly aggravated HFD-induced lipid elevation, while miR-320a inhibition had the opposite effect (Figures 2B and 2C). Correspondingly, lipid profiling of fast protein liquid chromatography (FPLC)-separated lipoprotein fractions showed that between-group differences in plasma TG were predominantly associated with very low-density lipoprotein particles (Figure 2D). This analysis also revealed higher cholesterol levels of LDL particles in HFD mice than in ND mice; miR-320a overexpression further elevated LDL-C, while miR-320a inhibition decreased LDL-C (Figure 2E).

Hepatic steatosis is closely associated with hyperlipidemia. Four weeks of HFD increased body weight, but altering miR-320a expression did not influence the body weight of HFD-treated mice (Figure S3B). HFD caused pale livers in mice without influencing liver weight (Figures S3C and S3D). Compared with control, rAAV-TBG-miR-320a treatment increased the severity of macrovesicular liver steatosis and elevated neutral hepatic lipid accumulation in HFD mice (Figures 2F and 2H). Total hepatic TG content also increased significantly in rAAV-TBG-miR-320a-treated versus rAAV-TBG-GFP-treated HFD mice (Figure 2G). Moreover, rAAV-TBG-anti-miR-320a treatment significantly reduced HFD-induced macrovesicular steatosis, neutral lipid accumulation, and TG content in the liver (Figures 2F–2H).

Together, these results demonstrate that liver-specific miR-320a overexpression aggravated HFD-induced hyperlipidemia and hepatic steatosis in mice.

miR-320a Overexpression Promoted TG Accumulation and Secretion and Reduced LDL Uptake in L02 Cells

Oleate and palmitate are the most abundant fatty acids in liver TG among both normal subjects and patients with fatty liver (Araya et al., 2004). We selected oleate for our experiments because palmitate is highly toxic and induces severe cell apoptosis. Oleic acid (OA) treatment significantly increased intracellular and medium TG in L02 cells (Figures 3A–3C). Similar to observations *in vivo*, miR-320a overexpression enhanced TG accumulation and secretion after OA treatment, while miR-320a inhibition caused the opposite effect (Figures 3A–3C).

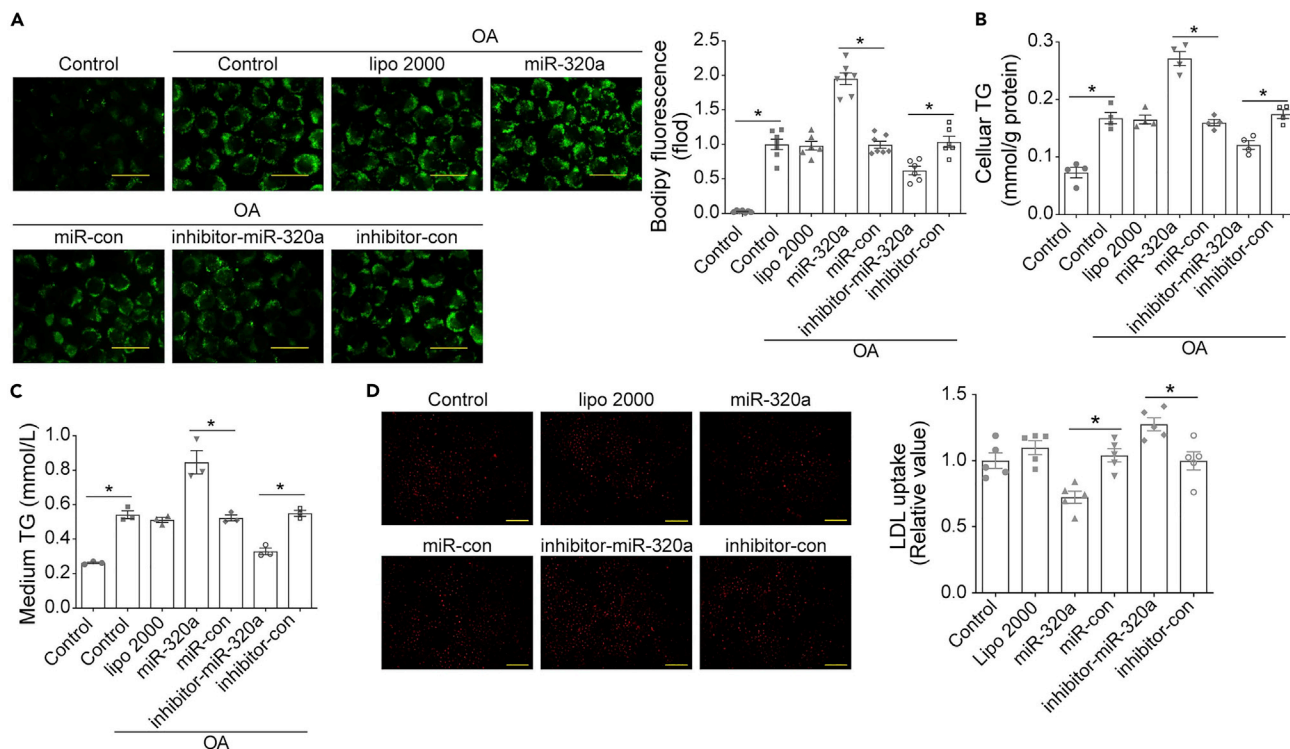


Figure 3. miR-320a Overexpression Promoted TG Accumulation and Secretion and Reduced LDL Uptake in L02 Cells

(A–C) L02 cells were transfected with miR-320a mimics/inhibitors (or their controls) and then subjected to 200 μ M oleic acid stimulation. (A) Representative images and quantitative analysis of BODIPY 493/503 fluorescent dye staining of neutral lipid in cells. Scale bar, 50 μ m ($n = 6$ –7 dishes per group). (B and C) Cellular (B) and medium (C) TG content of L02 cells with different treatment ($n = 4$ dishes per group for B; $n = 3$ dishes per group for C).

(D) L02 cells were transfected with miR-320a mimics/inhibitors (or their controls) and then subjected to pHrodo-Red-LDL (10 μ g/mL). Representative images and quantitative analysis of pHrodo-Red-LDL endocytosis in L02 cells ($n = 5$ dishes per group). Scale bar, 100 μ m. For (A–D), data are expressed as mean \pm SEM, * $p < 0.05$, Student's *t* test.

See also [Figures S4](#) and [S5](#), and [Table S4](#).

Hepatocyte uptake of LDL is the primary physiological process regulating plasma cholesterol content. Transfecting miR-320a mimics repressed LDL uptake in L02 cells. Conversely, miR-320a inhibitors promoted LDL uptake ([Figure 3D](#)).

To explore the underlying molecular mechanisms of miR-320a in hyperlipidemia, we performed RNA immunoprecipitation sequencing (RIP-seq) using anti-Argonaute2 (Ago2) antibody to identify the potential targets of miR-320a in L02 cells. Using a cutoff of fold change >2 and $p < 0.05$, we identified 43 mRNAs that showed increased association with the Ago2 protein after miR-320a transfection ([Figures S4A](#) and [S4B](#)), suggesting that miR-320a might enhance these mRNAs packaged into RNA-induced silencing complex. Then, we used the online computational tool, RNAhybrid, to screen the potential binding sites of miR-320a on these 43 mRNA sequences among human and mouse species ([Table S4](#)). Following a filtering criterion as minimum free energy lower than -20 Kcal/mol, 8 candidate genes—MAFB, ARHGAP31, GNAZ, TCF7, FAM13C, GLIS1, FAXC, and IDS—were identified as the potential targets of miR-320a in L02 cells. Among them, only the activity of luciferase reporter containing the 3' UTR sequence of MAFB, ARHGAP31, or TCF7 was obviously suppressed when co-transfected with miR-320a mimics, compared with miR-con ([Figure S4C](#)). Western blots were performed in L02 cells for further validation. miR-320a mimic transfection significantly reduced MafF and TCF7 protein levels ([Figures S4D](#) and [S4E](#)). These data indicated that MAFB and TCF7 were targets of miR-320a in L02 cells.

miR-320a is Linked to GWAS-Identified SNP rs12541335, Associated with Hypertriglyceridemia

We reasoned that genetic factors likely influence hyperlipidemia-associated abnormal miR-320a concentrations because high-fat treatments had no effect on hepatic miR-320a expression *in vivo* and *in vitro*

(Figures 2A and S5). Furthermore, plasma lipid level is a highly heritable quantitative trait. We also hypothesized that distal variants contribute to altered miR-320a expression because no evidence suggests that such variants are actually located in MIR320A. We first used the NHGRI-EBI GWAS Catalog to extract GWAS-identified significant single nucleotide polymorphisms (SNPs) in a 1 Mb region around MIR320A (Figure S6A and Table S5). Of the 28 SNPs, rs12541335 was significantly ($P = 7 \times 10^{-6}$) associated with hypertriglyceridemia in individuals of Mexican ancestry (odds ratio = 1.23, 95% CI = 1.13–1.33) (Weissglas-Volkov et al., 2013). Rs12541335 is a noncoding variant, and its loci (SFTPC, REEP4, POLR3D, PIWIL2, PHYHIP, LGI3, and BMP1) do not contain an obvious protein-coding gene implicated in hypertriglyceridemia. Using Encyclopedia of DNA Elements (ENCODE) ChIP-seq data, we further found that rs12541335 overlaps with H3K27me3 peaks in both human liver tissue and HepG2 cell line (Figure S6A). This result suggests that rs12541335 may be present in a distal regulatory element. Taken together, rs12541335 may be associated with miR-320a dysregulation in hyperlipidemia.

To determine whether rs12541335 and surrounding regions distantly targeted MIR320A, we performed 3C using an anchor primer within the restriction fragment of MIR320A promoter and primers spanning the region flanking MIR320A. The restriction fragment containing rs12541335 frequently interacted with MIR320A promoter in hepG2 and L02 cell lines (Figure 4A). For functional characterization, we employed real-time polymerase chain reaction (PCR) using multiple primer pairs to measure chromatin openness and histone markers (Figure S6B). Chromatin openness is related to the presence of regulatory elements (Bell et al., 2011). Heterochromatin is inaccessible to Dnase digestion, resulting in nonsignificant cycle-threshold (CT) shifts between Dnase-cut and uncut samples in CHART-PCR. In contrast, euchromatin is digestible and generates large CT shifts. As expected, the rs12541335-containing fragment exhibited high accessibility in hepG2 and L02 cell types (Figure S6C). The results of ChIP-qPCR indicated that H3k27me3 exhibited a high chromatin modification signal around rs12541335 in both cell lines. Thus, the rs12541335-containing fragment may be a putative regulatory element (PRE) of MIR320A (Figure S6D).

Luciferase reporter assays revealed successful induction of luciferase activity by MIR320A promoter in hepG2 and L02 cells. In stark contrast, PRE significantly reduced MIR320A promoter-driven luciferase activity (Figure 4B), indicating that the rs12541335-containing fragment acted as a transcriptional silencer of MIR320A.

Risk Allele of rs13282783 Reduced the Silencing Effect on MIR320A Promotor via Disrupting ZFP161 and HDAC2 Binding

Recent studies suggest that causal SNPs are more likely to be in linkage disequilibrium (LD) with the tag SNP (Freedman et al., 2011). Here, we used an LD cutoff of $r^2 \geq 0.2$ because GWAS may underestimate the strength of correlations between the associated and causal SNPs (Freedman et al., 2011). Otherwise, risk alleles of candidate causal SNPs are typically functional and could affect transcription factor binding. We thus generated a list of potential regulatory SNPs (rs12541335 and linked SNPs in LD) using HaploReg (Table S6). Three SNPs were located in the silencer element (Table S6), in accordance with our hypothesis that the rs12541335-containing fragment is an MIR320A silencer. These were prioritized as candidates for a follow-up functional study.

We introduced alternative alleles of candidate SNPs into PRE for luciferase assays. Alternative allele rs13282783T significantly reduced PRE inhibitory effects on MIR320A promotor (Figures 5A and S7A) in L02 and hepG2 cells. However, alternative alleles of rs12541335 or rs12541373 had no obvious effects (Figures 5A and S7A). DNase I hypersensitive sites are markers of cis-regulatory elements (including promoters, enhancers, insulators, silencers, and locus control regions). ENCODE Consortium has profiled DNase I hypersensitive site (DHS) in over 100 cell types (Thurman et al., 2012), allowing researchers to compute Pearson correlation coefficients between all distal DHS and promotor DHS across these cell types. Strong correlations between the two is highly suggestive of distal regulatory elements controlling specific genes (Consortium, 2012; Thurman et al., 2012). We thus extracted distal DHS within ± 500 kb and highly correlated with MIR320A promotor DHS. Only rs13282783 was located in one of the resultant DHS (Figure S8 and Table S7) but not the other two SNPs. Therefore, rs13282783 likely plays a role in miR-320a transcription.

As DHS typically indicates protein binding sites, we examined whether the C/T polymorphism at rs13282783 affected DNA-protein interactions. In silico bioinformatic analyses predicted that rs13282783 is involved in several position weight matrices (Table S8). We then performed electrophoretic mobility shift

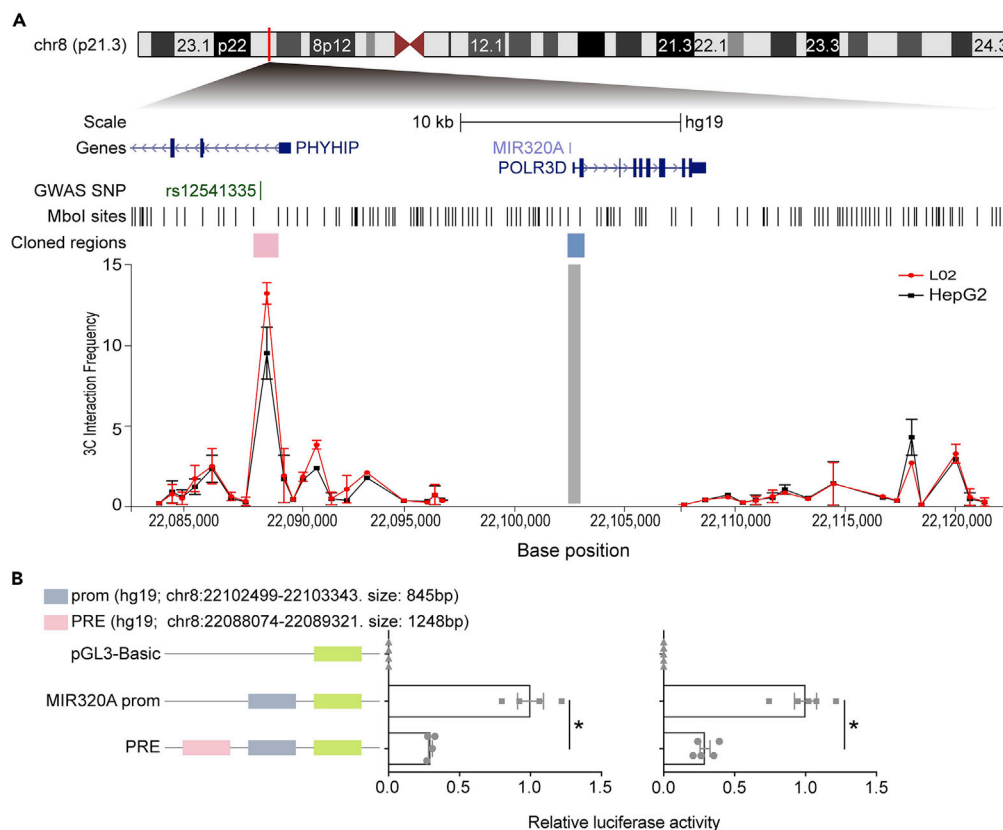


Figure 4. rs12541335 Association Region Acts as a Silencer Element of MIR320A

(A) 3C analysis of long-range interactions within a 40 kb region flanking MIR320A ($n = 2$ independent experiments). The chromosome, scale, genes, GWAS SNP, and Mbol sites at the top are based on the UCSC genome browser (human genome, version hg19; chromosome 8, nucleotides 22,082,475-22,122,556). The Mbol sites track shows the location of restriction enzyme Mbol recognition sites (black bars). The 3C interaction profiles in HepG2 and L02 hepatic cell lines are shown at the bottom. 3C libraries were generated with Mbol, with the anchor point set (gray box) at the MIR320A promoter region. A peak of interaction with MIR320A was observed for the fragment containing rs12541335 in both cell lines. Regions cloned into pGL3 reporter gene constructs are shown as pink and blue horizontal boxes, respectively. (B) Luciferase reporter assays following transient transfection in L02 (left) and HepG2 (right) cells ($n = 3$ independent experiments). The putative regulatory element (PRE, pink box) was cloned upstream of MIR320A promoter (blue box)-driven luciferase constructs. Data are expressed as mean \pm SEM, * $p < 0.05$, Student's *t* test.

See also [Figure S6](#), [Tables S5–S7](#).

assays using biotin-labeled oligonucleotide probes and L02 nuclear extracts. Gel shift results showed that the probe carrying the reference allele at rs13282783 interacted strongly with the nuclear extract. However, this interaction was significantly reduced for the probe with the alternative allele, suggesting a disruption of L02 nuclear protein binding to DNA ([Figures 5B](#) and [S9A](#)). We therefore excluded Gm397 because it was predicted to prefer binding to the alternative allele of rs13282783 ([Table S8](#)). Competition assays with standard sequences of predicted TF binding sites suggested that ZFP161 bound to DNA at rs13282783 ([Figures 5B](#) and [S9B](#)). No other standard TF sequences (including Egr-1, Pax-5, and ZBTB33) competed for binding to nuclear extract ([Figure S9B](#)). The supershift assay validated these results, showing that the nuclear protein binding to rs13282783 was most likely ZFP161 ([Figure 5B](#)).

ZFP161 typically acts as a transcriptional repressor ([Orlov et al., 2007](#)). Rs13282783 lies within the ZFP161 consensus binding sites. Given the strong preference for the reference allele at position 8 (log-odds score of 12.2), we predicted that altering the risk allele would severely affect binding affinity (log-odds score of 8.8) ([Figure 5C](#)). To determine whether ZFP161 mediates the effect of rs13282783, we performed a shRNA-mediated gene silencing study in L02 and HepG2 cells. ZFP161 silencing repressed PRE silencer activity on MIR320A promoter but had no such effect in either cell type when rs13282783T was present ([Figures 5D](#) and

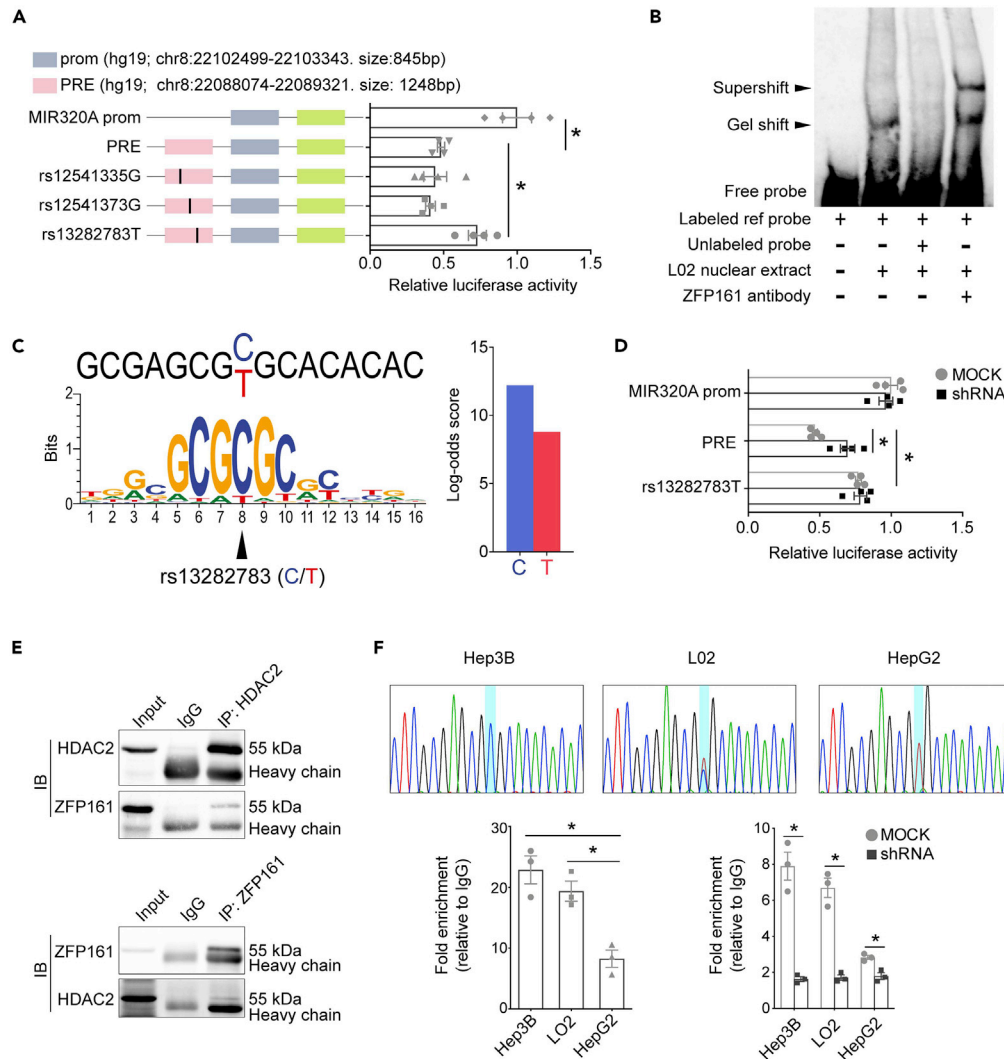


Figure 5. The Risk Allele of rs13282783 Reduced the Effect of the Silencer Element on MIR320A Promotor via Disrupting ZFP161 and HDAC2 Binding

(A) Luciferase reporter assays following transient transfection in L02 cells (n = 4 independent experiments). Alternative alleles (black bars) were engineered into the constructs which are denoted by corresponding SNP ID.

(B) Electrophoretic mobility shift assays (EMSA) using L02 nuclear proteins. Oligonucleotide probes for different alleles of rs13282783 were incubated with L02 nuclear extracts. The arrowheads indicate the gel-shift band of protein-DNA complexes and the supershift band of antibody-protein-DNA complexes. Unlabeled probe was used at 100-fold molar excess as a competitor of a labeled probe to demonstrate the specific binding at rs13282783.

(C) The rs13282783-T is predicted to disrupt a ZFP161 binding site. The 16 bp fragment surrounding rs13282783 and position-weight-matrix data of ZFP161 were shown on the left. The arrowhead indicates that rs13282783 is located at position 8. The log-odds score barplot (right) showing differential binding of ZFP161 at rs13282783.

(D) Luciferase reporter assays following transient transfection of corresponding constructs in L02 cells pre-treated with shRNA against ZFP161 (n = 4 independent experiments).

(E) Immunoprecipitation with the anti-ZFP161 (top) or anti-HDAC2 antibody (bottom) in L02 cells, followed by Western blotting with antibodies for anti-ZFP161 and anti-HDAC2.

(F) ChIP-qPCR on the region around rs13282783 in L02, HepG2, and Hep3B cells (n = 3 independent experiments). Sanger sequencing (top) of the PCR fragment generated using primers flanking rs13282783. The insert blue box highlights the homozygous TT genotype of rs13282783 in HepG2 cells, the heterozygous CT in L02 cells, and the homozygous CC in Hep3B cells. ChIP assays were performed with ZFP161 antibody (left at the bottom) or with HDAC2 antibody in cells pretreated with shRNA against ZFP161 and mock (right at the bottom). For (A), (D), and (F), data are expressed as mean \pm SEM, *p < 0.05, Student's t test.

See also [Figures S7–S9](#), [Tables S8](#) and [S9](#).

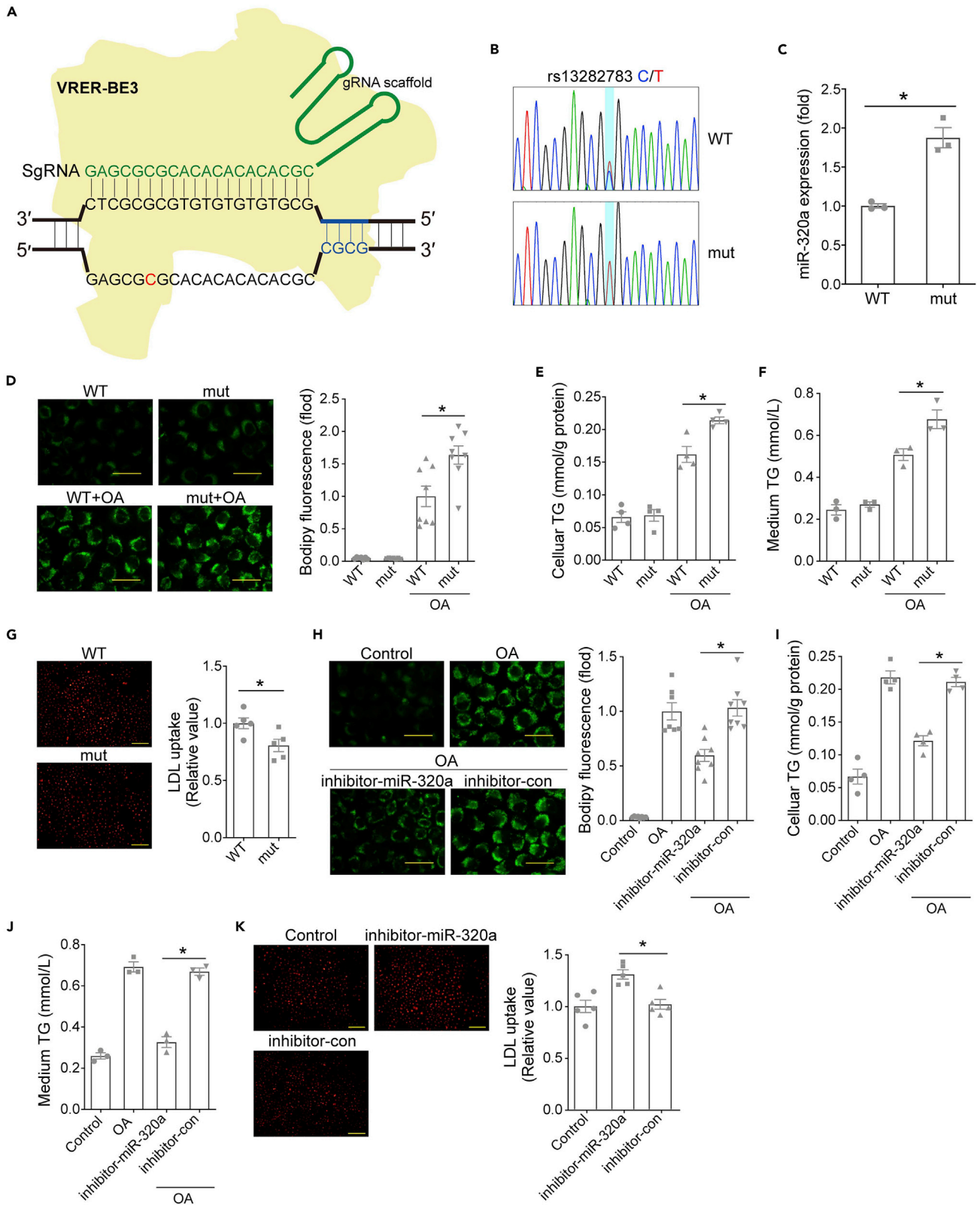


Figure 6. Base Editing of rs13282783 in L02 Cells Induced miR-320a Overexpression, Promoting TG Accumulation and Secretion and Reduced LDL Uptake

(A) VRER-BE3 targets sequence harboring rs13282783. DNA with rs13282783-C (red) specified by a guide RNA (gsRNA and gRNA scaffold, green) is bound by VRER-BE3 (light yellow), which recognize CGCG PAM (blue).
 (B) Sanger sequencing of the PCR fragment generated using primers flanking rs13282783 in wild-type and mutant L02 cells. The inset blue box highlights the homozygous TT genotype of rs13282783 in mutant HepG2 L02 cells and the heterozygous CT for wild-type L02 cells.
 (C) miR-320a expression was determined by real-time PCR in wild-type and mutant L02 cells (n = 3 independent experiments).
 (D–F) Wild-type and mutant L02 cells were subjected to oleic acid (200 $\mu\text{mol/L}$) stimulation. (D) Representative images and quantitative analysis of BODIBY 493/503 fluorescent dye staining of neutral lipid in cells (n = 7–8 dishes per group). Scale bar, 50 μm .
 (E and F) Cellular (E) and medium (F) TG content of wild-type and mutant L02 cells (n = 4 dishes per group for E; n = 3 dishes per group for F).
 (G) Wild-type and mutant L02 cells were subjected to pHrodo-Red-LDL (10 $\mu\text{g/mL}$). Representative images and quantitative analysis of pHrodo-Red-LDL endocytosis in L02 cells (n = 5 dishes per group). Scale bar, 100 μm .
 (H–J) Mutant L02 cells were transfected with miR-320a inhibitors or negative control and then subjected to oleic acid (200 $\mu\text{mol/L}$) stimulation. (H) Representative images and quantitative analysis of BODIBY 493/503 fluorescent dye staining of neutral lipid in cells (n = 7–8 dishes per group). Scale bar, 50 μm . (I and J) Cellular (I) and medium (J) TG content of mutant L02 cells with different treatment (n = 4 dishes per group for I; n = 3 dishes per group for J).
 (K) L02 cells were transfected with miR-320a mimics/inhibitors (or their controls) and then subjected to pHrodo-Red-LDL (10 $\mu\text{g/mL}$). Representative images and quantitative analysis of pHrodo-Red-LDL endocytosis in L02 cells (n = 5 dishes per group). Scale bar, 100 μm . Data are expressed as mean \pm SEM, *p < 0.05, Student's t test.

See also [Figures S10–S12](#) and [Data S1](#) and [S2](#).

S7B). Although HDAC2 is not a TF, rs13282783 alleles were also predicted to affect its DNA-binding ability. HDAC2 is a class I histone deacetylase (HDAC) that catalytically removes acetyl groups from specific lysine residues in the tails of core histones (Nakano et al., 2018). HDACs form transcriptional repressor complexes with numerous TFs (Nakano et al., 2018). As we predicted, co-immunoprecipitation assays showed that HDAC2 interacted with ZFP161 in L02 and HepG2 cells (Figures 5E and S7C). To further explore whether rs13282783 affects chromatin-bound ZFP161 and HDAC2 in hepatic cells, we sequenced several human hepatoma cell lines (including Hep3B, HepG2, L02, SMMC-7721, Bel7402, Huh7, HLE, and SNU-398; see [Table S9](#) for molecular characteristics). Our analysis revealed the homozygous TT genotype of rs13282783 in HepG2 cells, heterozygous CT in L02 cells, and homozygous CC in Hep3B cells (Figure 5F). Chromatin immunoprecipitation (ChIP) assays in these three cell lines confirmed ZFP161 and HDAC2 presence at rs13282783 (Figure 5F). Compared with TT-genotype HepG2 cells, CC or CT-genotype Hep3B and L02 cells showed greater ZFP161 and HDAC2 enrichment around rs13282783. This outcome suggests that chromatin binding of ZFP161 and HDAC2 favored the reference allele of rs13282783C (Figure 5F). Furthermore, ZFP161 silencing abolished HDAC2 enrichment at rs13282783 in all three cell types, demonstrating that ZFP161 is indispensable for HDAC2 recruitment to chromatin surrounding rs13282783 (Figure 5F).

We analyzed the association between rs13282783 polymorphisms and plasma lipid concentrations in 3000 unrelated individuals of Chinese Han descent. We found significant differences in plasma TG, LDL-C, and TC levels among the CC, CT, and TT genotype subgroups (Table S10). Furthermore, the proportion of a 1-SD change in plasma TG, LDL-C, and TC levels for each copy of the risk allele was 0.112, 0.096 and 0.097, respectively (Table S11).

Base Editing of rs13282783 in L02 Cells Induced miR-320a Overexpression, Promoting TG Accumulation and Secretion and Reduced LDL Uptake

Because L02, HepG2, and Hep3B vary considerably in their molecular characteristics (Table S9), naturally occurring rs13282783 polymorphisms in these cell types are unsuitable for evaluating correlations between genotype and miR-320a expression. We instead used base editing, a high-precision genome editing technique based on CRISPR-Cas9 without double-stranded DNA cleavage. We chose VRER-BE3 as our base editor because it can introduce C-to-T changes at desired sites in the genome (Kim et al., 2017) (Figure 6A). Sanger sequencing verified that wild-type CT genotype of rs13282783 in L02 cells was successfully altered to mutant TT (Figure 6B). Mutant L02 cells with TT genotype expressed more miR-320a than the wild type (Figure 6C). The results of miRNA-seq showed that the expression levels of 37 miRNAs were changed in mutant L02 cells with TT genotype, compared with the wild-type cells (Figure S10). However, miR-320a expression (basemean value: 30,352) was the most markedly elevated one comparing with other miRNAs (basemean values vary between 15 and 5755), suggesting the specificity of mutation induced miR-320a expression (Data S1). Other miRNAs might involve in the regulation network of miR-320a-related signals. The results of mRNA-seq showed 459 differentially expressed mRNAs between mutant and wild-type cells (Data S2), but the adjacent gene expression levels were not significantly changed (Figures S11A and S11B). KEGG (Kyoto Encyclopedia of Genes and Genomes) enrichment analysis of differentially expressed genes

in mRNA-seq showed several relevant pathways to lipid metabolism, including PPAR (peroxisome proliferator-activated receptor) signaling pathway, ABC (ATP-binding cassette) transporters, advanced glycation end products (AGEs) and their receptors (RAGEs) signaling pathway in diabetic complications, and PI3K (phosphatidylinositol 3 kinase)-Akt (protein kinase B) signaling pathway (Figure S11C). Furthermore, compared with wild-type cells, the mutant L02 cells showed decreased binding of ZFP161 with the PRE fragment and expressed reduced protein levels of MAFB and TCF7, which were the targets of miR-320a (Figure S12). Moreover, intracellular and medium TG was higher in mutant versus wild-type cells after OA treatment (Figures 6D–6F). Mutants also exhibited lower LDL uptake (Figure 6G). Notably, miR-320a inhibitor reversed all of these effects (Figures 6H–6K). Our findings indicated that base editing of rs13282783 (from CT to TT) in L02 cells induced miR-320a overexpression, thereby aggravating OA-induced TG accumulation and secretion, as well as reducing LDL uptake.

DISCUSSION

Here, we successfully showed that the risk allele of GWAS-identified SNP rs13282783 contributed to hyperlipidemia by upregulating miR-320a expression. Firstly, we found a tight link between hyperlipidemia and increased plasma miR-320a levels in a general population. To establish the potential causal effect, we performed rAAV-mediated loss- and gain-of-function studies in the mouse liver, revealing that elevated miR-320a is sufficient to aggravate diet-induced hyperlipidemia and hepatic steatosis. We further demonstrated that miR-320a promoted triglyceride accumulation and secretion and reduced LDL uptake in liver cells. Through an analysis of available GWAS data and epigenetic profiles in relevant cell types, we identified SNP rs12541335 associated with hyperlipidemia, which resides in a putative silencer element for the MIR320A gene. Linkage analyses and functional studies then demonstrated that the rs13282783 T allele indeed obligated the silencer activity by preventing the repressor ZFP161 and corepressor HDAC2 from binding to DNA that led to miR-320a upregulation. We further confirmed this genetic connection on an independent patient population and through direct genome editing in liver cells. Our studies provided further insight on the role of miRNA in controlling lipid homeostasis. We also advanced a new strategy for interpreting functional consequences of GWAS-implicated genetic variants.

Previously, we showed that patients with CAD and high-risk individuals exhibited markedly elevated plasma miR-320a (Chen et al., 2015). Elevated circulating miR-320a was also reported in individuals with insulin resistance, metabolic syndrome, and diabetes (Flowers et al., 2015; Karolina et al., 2012; Wang et al., 2014), risk factors of CAD. Here, our correlation analysis confirmed the role of miR-320a in CAD risk through identifying a positive correlation between plasma miR-320a and multiple metabolic parameters. After adjusting for BMI, miR-320a level remained significantly correlated with plasma lipids. Overall, these results suggested that elevated miR-320a was tightly linked with CAD risk factors, especially hyperlipidemia.

The main contributing tissue of the circulating miR-320a remains to be elucidated. The parent tissue could be obviously identified if the circulating tissue-specific miRNA (e.g. miR-122) is expressed (Dear et al., 2018). Circulating miRNAs are secreted into blood mainly in the following two ways: (1) encapsulated in lipid vesicles (such as exosomes, microvesicles, and apoptotic bodies) and (2) being associated with RNA binding proteins (such as NPM1 and Ago2) or lipoprotein complexes. Microvesicles and apoptotic bodies were formed by direct budding of the parent cell membrane (Huang-Doran et al., 2017). Thus, the main contributing tissue might also be identified according to the cargo of circulating miRNAs. However, miR-320a is expressed ubiquitously in multiple tissues and the cargo of circulating miR-320a is unclear; it is difficult to identify the main contributing tissue to the elevated circulating miR-320a in human patients. In animal studies, most of them investigated the roles of circulating miRNAs in the target recipient cells, only few of them focused on the main contributing tissues to the circulating miRNAs. Ronald Kahn's group reported that the levels of circulating miRNAs were decreased in the adipose tissue-specific Dicer-deficient mice, which were defective in miRNA processing specifically in the adipose tissue, suggesting that the adipose tissue might contribute to the circulating miRNAs in mice (Thomou et al., 2017). Therefore, tissue-specific miR-320a-deficient or -overexpressing mice models might be beneficial to demonstrate the main contributing tissues to the elevated plasma miR-320a, which needs further investigation.

When we manipulated hepatic miR-320a expression in HFD-fed mice, we observed that overexpression of miR-320a aggravated diet-induced hyperlipidemia and hepatic steatosis. Using Ago2 RIP-seq and biological validation, we found that MAFB and TCF7 were miR-320a targets in liver cells. These results are in line with previous research studies showing that MAFB and TCF7 are important regulators of metabolic

disorders (Kaur et al., 2015; Pettersson et al., 2015). However, the exact nature of MAFB and TCF7 involved in miR-320a controlling hyperlipidemia requires more data to confirm, which might be another interesting story.

In the current study, over-nutrient stimuli did not alter miR-320a expression in the liver tissue and cell lines. However, elevated hepatic miR-320a is sufficient to aggravate diet-induced hyperlipidemia through promoting triglyceride accumulation and secretion and reducing LDL uptake. Therefore, hepatic miR-320a overexpression led to hyperlipidemia, not vice versa.

Many studies suggest that besides environmental influence, genetic components inducing gene aberrant expression participates in the pathogenesis of various diseases (Duan et al., 2014; Mika and Lynch, 2016; Ye et al., 2016). Therefore, we reasoned that genetic factors likely influence hyperlipidemia-associated abnormal miR-320a concentrations, considering that high-fat treatments had no effect on hepatic miR-320a expression *in vivo* and *in vitro*. Then, we provided multiple lines of evidence to demonstrate that rs13282783T upregulates miR-320a expression in liver cells, thereby increasing hyperlipidemia susceptibility. Our results suggest that genetic factors participate in pathogenesis through inducing abnormal miRNA expression.

Natural genetic variation rarely occurs directly within miRNAs. Instead, quantitative trait locus (QTL) analyses showed that miRNA transcript abundance in multiple diseases (including hyperlipidemia) is associated with remote SNPs, called mirQTLs (Huan et al., 2015; Siddle et al., 2014; Wagschal et al., 2015). Recent studies speculated that trans-mirQTLs mainly exert their effect through affecting the stability of mature miRNA, while cis-mirQTLs appear to regulate the expression of miRNAs through affecting the activity of cis-elements (Nikpay et al., 2019; Suzuki et al., 2017). Nikpay et al. reported that rs34852232 was a strong trans-eQTL for miR-320a, b, c, d, e (they share similar mature sequences but vary in transcriptional regulatory elements) (Nikpay et al., 2019). Here, we found that rs13282783 was located in a silencer element of MIR320A and its T allele led to miR-320a overexpressing by decreasing the silencer activity. Our present study identified a cis-eQTL for miR-320a and elucidated the underlying mechanism.

In GWASs, hundreds of thousands of SNPs are assayed by high-throughput genotyping technologies (e.g. GWAS genotyping chips) to relate them to diseases and traits. To reduce the cost of GWASs and the redundant information, a subset of the SNPs, termed tag SNPs, is genotyped in practice (Pearson and Manolio, 2008). Tag SNPs are selected by utilizing the correlation structure between the SNPs, referred to as LD. GWAS genotyping chips were designed using tag SNPs to capture LD structure rather than causal SNPs themselves (Freedman et al., 2011). This means that the tag SNPs reported to be associated with a phenotype merely define a chromosomal region (typically defined as 500 kbp on either side of the tag SNP) where the causal variant may be located (Freedman et al., 2011). Therefore, the GWAS hit is giving a clue to capture the causal SNP, rather than the causal SNP itself. After identifying the GWAS hit, the next step will be using sophisticated bioinformatics tools such as ENCODE and a series of wet lab experiments to validate the causal SNPs. In the current study, we used the NHGRI-EBI GWAS Catalog to extract GWAS-identified significant SNPs in 500 kbp on either side of MIR320A and found a GWAS hit rs12541335 was significantly associated with hypertriglyceridemia. We identified the causal SNP rs13282783 in rs12541335 captured LD block through a series of analyses and biological experiments.

In conclusion, our results reveal that upregulated miR-320a frequently detected in patients with CAD plays a causal role in hyperlipidemia. Besides environmental influence, we established a genetic component in the regulation of miR-320a expression. These findings suggest a potential therapeutic avenue to treat CAD by blocking miR-320a in patient liver.

Limitations of the Study

We only employed GWAS data and ignored the rare SNPs (MAF <0.05) that could have stronger effects on disease susceptibility. To verify the significance of this genetic variant in human population, we analyzed the association between rs13282783 polymorphisms and the plasma lipid concentrations in 3000 unrelated individuals of Chinese Han descent and found that rs13282783 was a risk variant for hyperlipidemia susceptibility. However, our subjects from Central China might not be entirely representative of the Chinese Han population. Therefore, further research is still required to validate the significance of this genetic variant. Our *in vitro* experiments were limited to L02 and HepG2 cell lines. In the future, we should confirm these

findings in normal hepatocytes, such as those differentiated from induced pluripotent stem cells. Therefore, further research is also required to conclusively delineate whether and how a functional genetic variant increases miR-320a expression in hyperlipidemia.

Resource Availability

Lead Contact

Further information and requests for resources should be directed to and will be fulfilled by the Lead Contact, Chen Chen (chenchen@tjh.tjmu.edu.cn).

Materials Availability

This study did not generate new unique materials.

Data and Code Availability

All data produced or analyzed for this study are included in the published article and its [supplementary information](#) files. The accession numbers for the RNA-seq data reported in this paper are GSE160744, GSE160745, and GSE160746 in GEO, respectively.

METHODS

All methods can be found in the accompanying [Transparent Methods](#) supplemental file.

SUPPLEMENTAL INFORMATION

Supplemental Information can be found online at <https://doi.org/10.1016/j.isci.2020.101788>.

ACKNOWLEDGMENTS

We thank Prof. Xiangdong Fu for stimulating discussions and editing the manuscript during the course of this investigation. This work was supported by grants from the National Natural Science Foundation of China (nos. 81822002, 91839302, 81630010, 31771264, 81790624, 31800973, and 82000387) and the Fundamental Research Funds for the Central Universities (2019kfyXMBZ035).

AUTHORS CONTRIBUTION

Z.Y., Y.Z., and H.D. designed and performed all the experiments. X.N., H.L., and J.F. participated in *in vitro* assays. M.H., B.D., X.Z., S.Y., and Z.W. participated in *in vivo* assays. C.C. and D.W.W. designed the experiments and wrote the manuscript. All authors read and approved the final manuscript.

DECLARATION OF INTERESTS

The authors declare no competing interests.

Received: July 1, 2020

Revised: October 14, 2020

Accepted: November 6, 2020

Published: December 18, 2020

REFERENCES

- Araya, J., Rodrigo, R., Videla, L.A., Thielemann, L., Orellana, M., Pettinelli, P., and Poniachik, J. (2004). Increase in long-chain polyunsaturated fatty acid n - 6/n - 3 ratio in relation to hepatic steatosis in patients with non-alcoholic fatty liver disease. *Clin. Sci. (Lond)* 106, 635–643.
- Atanasovska, B., Kumar, V., Fu, J., Wijmenga, C., and Hofker, M.H. (2015). GWAS as a driver of gene discovery in cardiometabolic diseases. *Trends Endocrinol. Metab.* 26, 722–732.
- Bell, O., Tiwari, V.K., Thoma, N.H., and Schubeler, D. (2011). Determinants and dynamics of genome accessibility. *Nat. Rev. Genet.* 12, 554–564.
- Benjamin, E.J., Muntner, P., Alonso, A., Bittencourt, M.S., Callaway, C.W., Carson, A.P., Chamberlain, A.M., Chang, A.R., Cheng, S., Das, S.R., et al. (2019). Heart disease and stroke statistics-2019 update: a report from the American heart association. *Circulation* 139, e56–e528.
- Chen, C., Wang, Y., Yang, S., Li, H., Zhao, G., Wang, F., Yang, L., and Wang, D.W. (2015). MiR-320a contributes to atherogenesis by augmenting multiple risk factors and down-regulating SRF. *J. Cell Mol. Med.* 19, 970–985.
- Cohen, J.C. (2016). Using human genetics to discover new therapeutic targets for plasma lipids. *J. Intern. Med.* 280, 487–495.
- Consortium, C.A.D., Deloukas, P., Kanoni, S., Willenborg, C., Farrall, M., Assimes, T.L., Thompson, J.R., Ingelsson, E., Saleheen, D., Erdmann, J., et al. (2013). Large-scale association analysis identifies new risk loci for coronary artery disease. *Nat. Genet.* 45, 25–33.

Consortium, E.P. (2012). An integrated encyclopedia of DNA elements in the human genome. *Nature* 489, 57–74.

Dear, J.W., Clarke, J.I., Francis, B., Allen, L., Wraight, J., Shen, J., Dargan, P.I., Wood, D., Cooper, J., Thomas, S.H.L., et al. (2018). Risk stratification after paracetamol overdose using mechanistic biomarkers: results from two prospective cohort studies. *Lancet Gastroenterol. Hepatol.* 3, 104–113.

Du, M., Yuan, T., Schilter, K.F., Dittmar, R.L., Mackinnon, A., Huang, X., Tschannen, M., Worthey, E., Jacob, H., Xia, S., et al. (2015). Prostate cancer risk locus at 8q24 as a regulatory hub by physical interactions with multiple genomic loci across the genome. *Hum. Mol. Genet.* 24, 154–166.

Duan, J., Shi, J., Fiorentino, A., Leites, C., Chen, X., Moy, W., Chen, J., Alexandrov, B.S., Usheva, A., He, D., et al. (2014). A rare functional noncoding variant at the GWAS-implicated MIR137/MIR2682 locus might confer risk to schizophrenia and bipolar disorder. *Am. J. Hum. Genet.* 95, 744–753.

Flowers, E., Aouizerat, B.E., Abbasi, F., Lamendola, C., Grove, K.M., Fukuoka, Y., and Reaven, G.M. (2015). Circulating microRNA-320a and microRNA-486 predict thiazolidinedione response: moving towards precision health for diabetes prevention. *Metab. Clin. Exp.* 64, 1051–1059.

Freedman, M.L., Monteiro, A.N., Gayther, S.A., Coetzee, G.A., Risch, A., Plass, C., Casey, G., De Biasi, M., Carlson, C., Duggan, D., et al. (2011). Principles for the post-GWAS functional characterization of cancer risk loci. *Nat. Genet.* 43, 513–518.

Go, A.S., Mozaffarian, D., Roger, V.L., Benjamin, E.J., Berry, J.D., Borden, W.B., Bravata, D.M., Dai, S., Ford, E.S., Fox, C.S., et al. (2013). Heart disease and stroke statistics—2013 update: a report from the American Heart Association. *Circulation* 127, e6–e245.

Hammond, S.M. (2015). An overview of microRNAs. *Adv. Drug Deliv. Rev.* 87, 3–14.

Hanin, G., Yayon, N., Tzur, Y., Haviv, R., Bennett, E.R., Udi, S., Krishnamoorthy, Y.R., Kotsiliti, E., Zangen, R., Efron, B., et al. (2018). miRNA-132 induces hepatic steatosis and hyperlipidaemia by synergistic multitarget suppression. *Gut* 67, 1124–1134.

Hayashi, M., Jin, Y., Yorgov, D., Santorico, S.A., Hagman, J., Ferrara, T.M., Jones, K.L., Cavalli, G., Dinarello, C.A., and Spritz, R.A. (2016). Autoimmune vitiligo is associated with gain-of-function by a transcriptional regulator that elevates expression of HLA-A*02:01 in vivo. *Proc. Natl. Acad. Sci. U S A* 113, 1357–1362.

Huan, T., Rong, J., Liu, C., Zhang, X., Tanriverdi, K., Joehanes, R., Chen, B.H., Murabito, J.M., Yao, C., Courchesne, P., et al. (2015). Genome-wide identification of microRNA expression quantitative trait loci. *Nat. Commun.* 6, 6601.

Huang-Doran, I., Zhang, C.-Y., and Vidal-Puig, A. (2017). Extracellular vesicles: novel mediators of cell communication in metabolic disease. *Trends Endocrinol. Metab.* 28, 3–18.

Karolina, D.S., Tavintharan, S., Armugam, A., Sepramaniam, S., Pek, S.L.T., Wong, M.T.K., Lim, S.C., Sum, C.F., and Jeyaseelan, K. (2012). Circulating miRNA profiles in patients with metabolic syndrome. *J. Clin. Endocr. Metab.* 97, E2271–E2276.

Kaur, K., Vig, S., Srivastava, R., Mishra, A., Singh, V.P., Srivastava, A.K., and Datta, M. (2015). Elevated hepatic miR-22-3p expression impairs gluconeogenesis by silencing the Wnt-responsive transcription factor Tcf7. *Diabetes* 64, 3659–3669.

Kim, Y.B., Komor, A.C., Levy, J.M., Packer, M.S., Zhao, K.T., and Liu, D.R. (2017). Increasing the genome-targeting scope and precision of base editing with engineered Cas9-cytidine deaminase fusions. *Nat. Biotechnol.* 35, 371–376.

Maurano, M.T., Humbert, R., Rynes, E., Thurman, R.E., Haugen, E., Wang, H., Reynolds, A.P., Sandstrom, R., Qu, H., Brody, J., et al. (2012). Systematic localization of common disease-associated variation in regulatory DNA. *Science* 337, 1190–1195.

Mika, K.M., and Lynch, V.J. (2016). An ancient fecundability-associated polymorphism switches a repressor into an enhancer of endometrial TAP2 expression. *Am. J. Hum. Genet.* 99, 1059–1071.

Nakano, Y., Kelly, M.C., Rehman, A.U., Boger, E.T., Morell, R.J., Kelley, M.W., Friedman, T.B., and Banfi, B. (2018). Defects in the alternative splicing-dependent regulation of REST cause deafness. *Cell* 174, 536–548 e521.

Nikpay, M., Beehler, K., Valsesia, A., Hager, J., Harper, M.E., Dent, R., and McPherson, R. (2019). Genome-wide identification of circulating-miRNA expression quantitative trait loci reveals the role of several miRNAs in the regulation of cardiometabolic phenotypes. *Cardiovasc. Res.* 115, 1629–1645.

Orlov, S.V., Kuteykin-Teplyakov, K.B., Ignatovich, I.A., Dizhe, E.B., Mirgorodskaya, O.A., Grishin, A.V., Guzhova, O.B., Prokhortchouk, E.B., Guliy, P.V., and Perevozchikov, A.P. (2007). Novel repressor of the human FMR1 gene - identification of p56 human (GCC)(n)-binding protein as a Kruppel-like transcription factor ZF5. *FEBS J.* 274, 4848–4862.

Painter, J.N., Kaufmann, S., O'Mara, T.A., Hillman, K.M., Sivakumaran, H., Darabi, H., Cheng, T.H.T., Pearson, J., Kazakoff, S., Waddell, N., et al. (2016). A common variant at the 14q32 endometrial cancer risk locus activates AKT1 through YY1 binding. *Am. J. Hum. Genet.* 98, 1159–1169.

Pearson, T.A., and Manolio, T.A. (2008). How to interpret a genome-wide association study. *JAMA* 299, 1335–1344.

Pettersson, A.M., Acosta, J.R., Bjork, C., Kratzel, J., Stenson, B., Blomqvist, L., Viguerie, N., Langin, D., Arner, P., and Laurencikienė, J. (2015). MAFB as a novel regulator of human adipose tissue inflammation. *Diabetologia* 58, 2115–2123.

Rayner, K.J., Suarez, Y., Davalos, A., Parathath, S., Fitzgerald, M.L., Tamahiro, N., Fisher, E.A., Moore, K.J., and Fernandez-Hernando, C. (2010). MiR-33 contributes to the regulation of cholesterol homeostasis. *Science* 328, 1570–1573.

Sabatti, C., Service, S.K., Hartikainen, A.L., Pouta, A., Ripatti, S., Brodsky, J., Jones, C.G., Zaitlen, N.A., Varilo, T., Kaakinen, M., et al. (2009). Genome-wide association analysis of metabolic traits in a birth cohort from a founder population. *Nat. Genet.* 41, 35–46.

Sadiq, S., Crowley, T.M., Charchar, F.J., Sanigorski, A., and Lewandowski, P.A. (2017). MicroRNAs in a hypertrophic heart: from foetal life to adulthood. *Biol. Rev. Camb. Philos. Soc.* 92, 1314–1331.

Siddle, K.J., Deschamps, M., Tailleur, L., Nedelec, Y., Pothlichet, J., Lugo-Villarino, G., Libri, V., Gicquel, B., Neyrolles, O., Laval, G., et al. (2014). A genomic portrait of the genetic architecture and regulatory impact of microRNA expression in response to infection. *Genome Res.* 24, 850–859.

Suzuki, H.I., Young, R.A., and Sharp, P.A. (2017). Super-enhancer-mediated RNA processing revealed by integrative MicroRNA network analysis. *Cell* 168, 1000–1014 e1015.

Teslovich, T.M., Musunuru, K., Smith, A.V., Edmondson, A.C., Stylianou, I.M., Koseki, M., Pirruccello, J.P., Ripatti, S., Chasman, D.I., Willer, C.J., et al. (2010). Biological, clinical and population relevance of 95 loci for blood lipids. *Nature* 466, 707–713.

Thomou, T., Mori, M.A., Dreyfuss, J.M., Konishi, M., Sakaguchi, M., Wolfrum, C., Rao, T.N., Winnay, J.N., Garcia-Martin, R., Grinspoon, S.K., et al. (2017). Adipose-derived circulating miRNAs regulate gene expression in other tissues. *Nature* 542, 450–455.

Thurman, R.E., Rynes, E., Humbert, R., Vierstra, J., Maurano, M.T., Haugen, E., Sheffield, N.C., Stergachis, A.B., Wang, H., Vernot, B., et al. (2012). The accessible chromatin landscape of the human genome. *Nature* 489, 75–82.

Turcot, V., Lu, Y., Highland, H.M., Schurmann, C., Justice, A.E., Fine, R.S., Bradfield, J.P., Esko, T., Giri, A., Graff, M., et al. (2018). Protein-altering variants associated with body mass index implicate pathways that control energy intake and expenditure in obesity. *Nat. Genet.* 50, 26–41.

Visscher, P.M., Wray, N.R., Zhang, Q., Sklar, P., McCarthy, M.I., Brown, M.A., and Yang, J. (2017). 10 Years of GWAS discovery: biology, function, and translation. *Am. J. Hum. Genet.* 101, 5–22.

Wagschal, A., Najafi-Shoushtari, S.H., Wang, L., Goedeke, L., Sinha, S., deLemos, A.S., Black, J.C., Ramirez, C.M., Li, Y., Tewhey, R., et al. (2015). Genome-wide identification of microRNAs regulating cholesterol and triglyceride homeostasis. *Nat. Med.* 21, 1290–1297.

Wahl, S., Drong, A., Lehne, B., Loh, M., Scott, W.R., Kunze, S., Tsai, P.C., Ried, J.S., Zhang, W., Yang, Y., et al. (2017). Epigenome-wide association study of body mass index, and the adverse outcomes of adiposity. *Nature* 541, 81–86.

Wang, X., Sundquist, J., Zoller, B., Memon, A.A., Palmer, K., Sundquist, K., and Bennet, L. (2014). Determination of 14 circulating microRNAs in Swedes and Iraqis with and without diabetes mellitus type 2. *PLoS one* 9, e86792.

Weissglas-Volkov, D., Aguilar-Salinas, C.A., Nikkola, E., Deere, K.A., Cruz-Bautista, I., Arellano-Campos, O., Munoz-Hernandez, L.L., Gomez-Munguia, L., Ordonez-Sanchez, M.L., Reddy, P.M., et al. (2013). Genomic study in Mexicans identifies a new locus for triglycerides and refines European lipid loci. *J. Med. Genet.* 50, 298–308.

Willer, C.J., Schmidt, E.M., Sengupta, S., Peloso, G.M., Gustafsson, S., Kanoni, S., Ganna, A., Chen, J., Buchkovich, M.L., Mora, S., et al. (2013). Discovery and refinement of loci associated with lipid levels. *Nat. Genet.* 45, 1274–1283.

Xie, M., Li, M., Vilborg, A., Lee, N., Shu, M.D., Yartseva, V., Sestan, N., and Steitz, J.A. (2013). Mammalian 5'-capped microRNA precursors that generate a single microRNA. *Cell* 155, 1568–1580.

Ye, J., Tucker, N.R., Weng, L.-C., Clauss, S., Lubitz, S.A., and Ellinor, P.T. (2016). A functional variant associated with atrial fibrillation regulates PITX2c expression through TFAP2a. *Am. J. Hum. Genet.* 99, 1281–1291.

Yusuf, S., Hawken, S., Ounpuu, S., Dans, T., Avezum, A., Lanas, F., McQueen, M., Budaj, A., Pais, P., Varigos, J., et al. (2004). Effect of potentially modifiable risk factors associated with myocardial

infarction in 52 countries (the INTERHEART study): case-control study. *Lancet* 364, 937–952.

Zhang, X.R., Zuo, X.X., Yang, B., Li, Z.R., Xue, Y.C., Zhou, Y., Huang, J., Zhao, X.L., Zhou, J., Yan, Y., et al. (2014). MicroRNA directly enhances mitochondrial translation during muscle differentiation. *Cell* 158, 607–619.

Zhao, Y., Yin, Z., Li, H., Fan, J., Yang, S., Chen, C., and Wang, D.W. (2017). MiR-30c protects diabetic nephropathy by suppressing epithelial-to-mesenchymal transition in db/db mice. *Aging Cell* 16, 387–400.

iScience, Volume 23

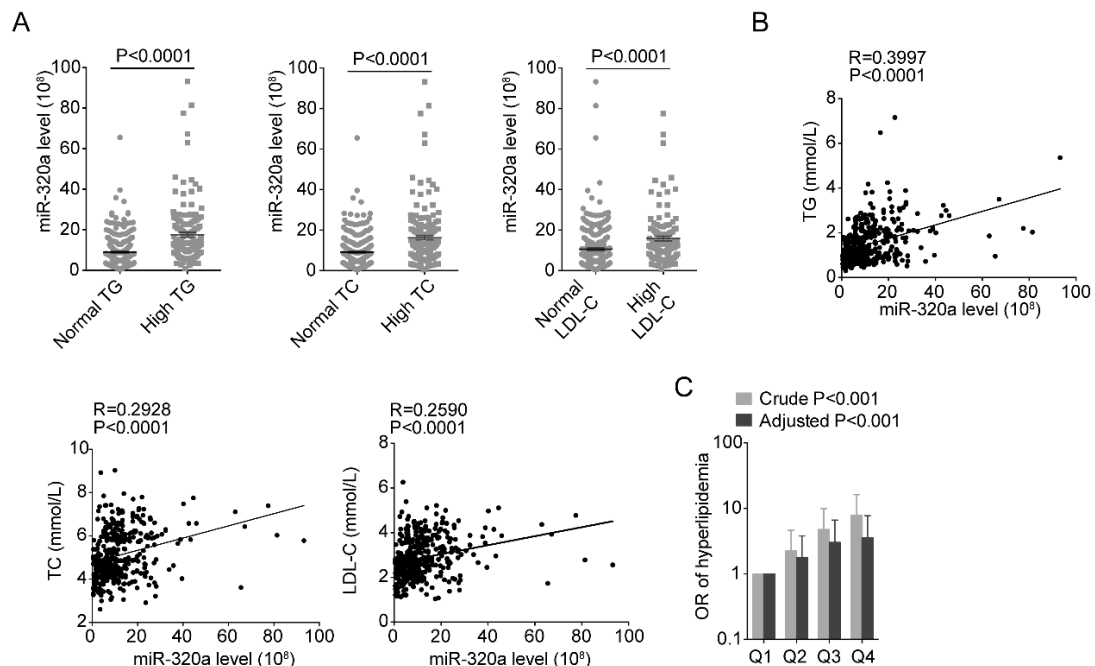
Supplemental Information

A Key GWAS-Identified Genetic Variant Contributes to Hyperlipidemia by Upregulating miR-320a

Zhongwei Yin, Yanru Zhao, Hengzhi Du, Xiang Nie, Huaping Li, Jiahui Fan, Mengying He, Beibei Dai, Xudong Zhang, Shuai Yuan, Zheng Wen, Chen Chen, and Dao Wen Wang

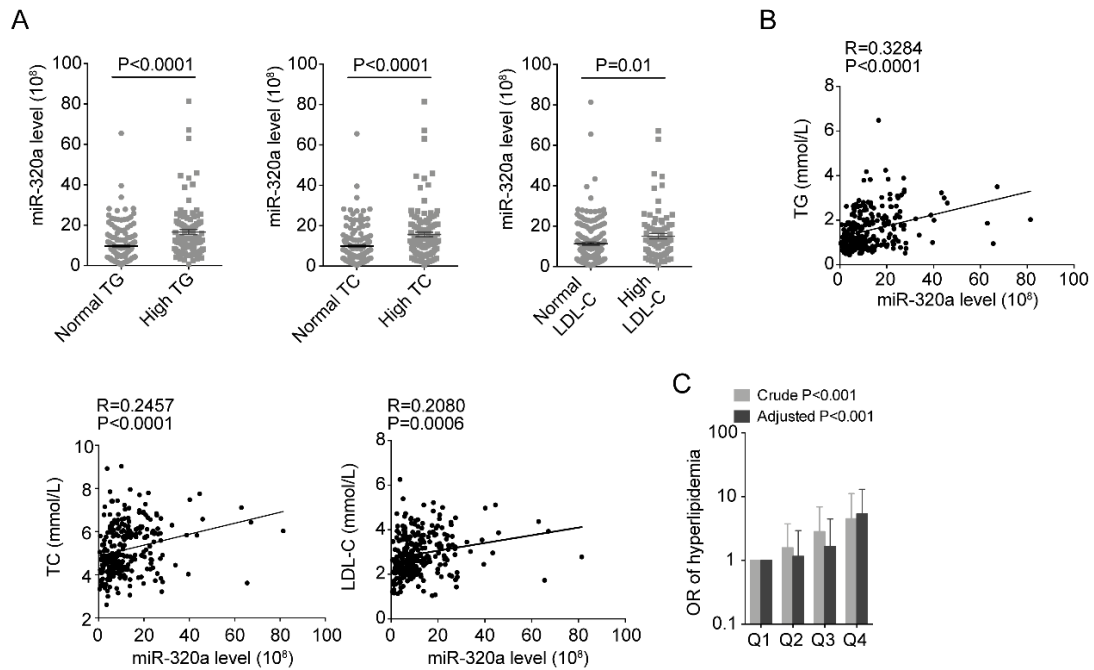
Figure S1. Circulating miR-320a level was elevated in hyperlipemia, Related to the Figure

1.



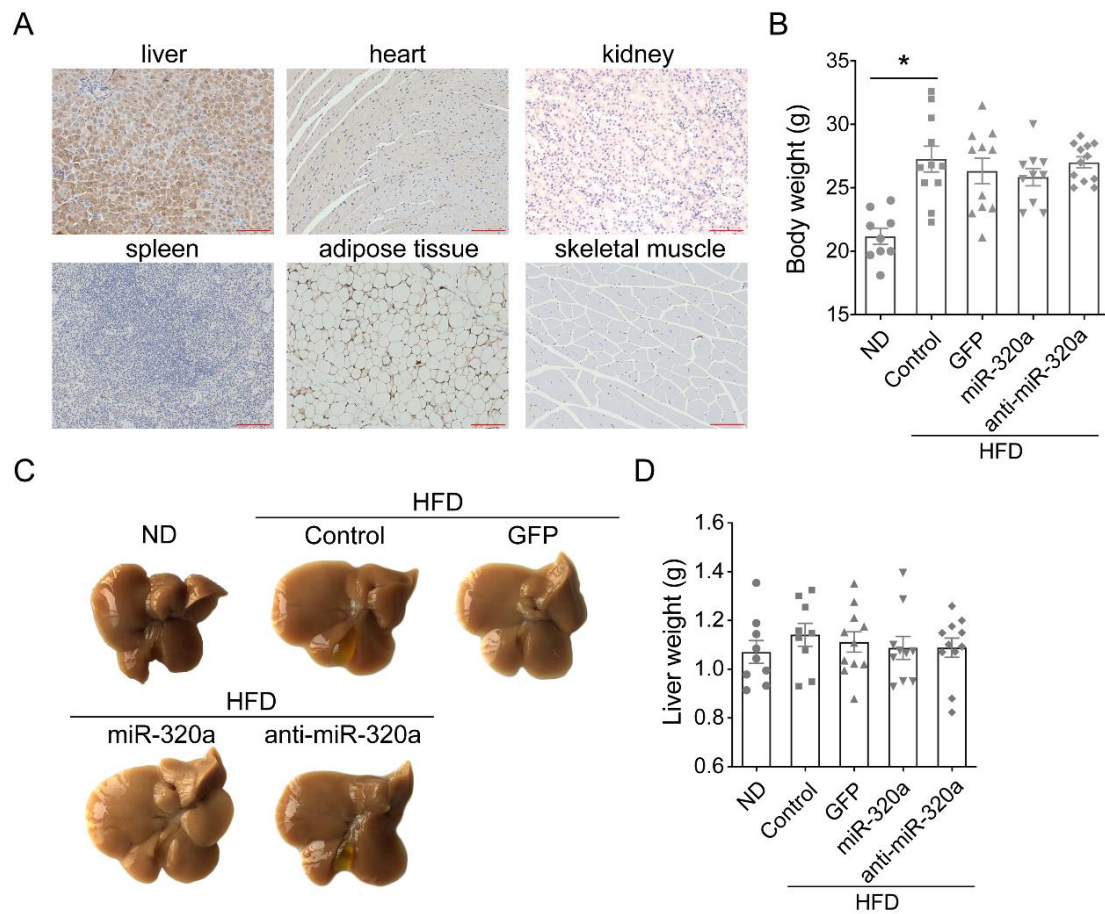
(A) The levels of circulating miR-320a in people with normal and high TG, normal and high TC as well as normal and high LDL-C ($n = 254$ for normal TG; $n = 150$ for high TG; $n = 235$ for normal TC; $n = 169$ for high TC; $n = 286$ for normal LDL-C; $n = 118$ for high LDL-C. Data are expressed as mean \pm SEM, Student's t test). (B) The correlation of circulating miR-320a levels with TG, TC or LDL-C ($n = 404$. The P values were produced by Pearson correlation analysis). (C) ORs (crude or adjusted for BMI) of hyperlipidemia stratified by quartile level of circulating miR-320a ($n = 404$. Logistic regression with and without adjustment for BMI was used and data are expressed as ORs and their 95% CIs). Q1, first quartile; Q2, second quartile; Q3, third quartile; Q4, fourth quartile. TG indicates triglyceride; TC, total cholesterol; LDL-C, low density lipoprotein cholesterol; CI, confidence interval; OR, odds ratio.

Figure S2. Circulating miR-320a level was elevated in women with hyperlipemia, Related to the Figure 1.



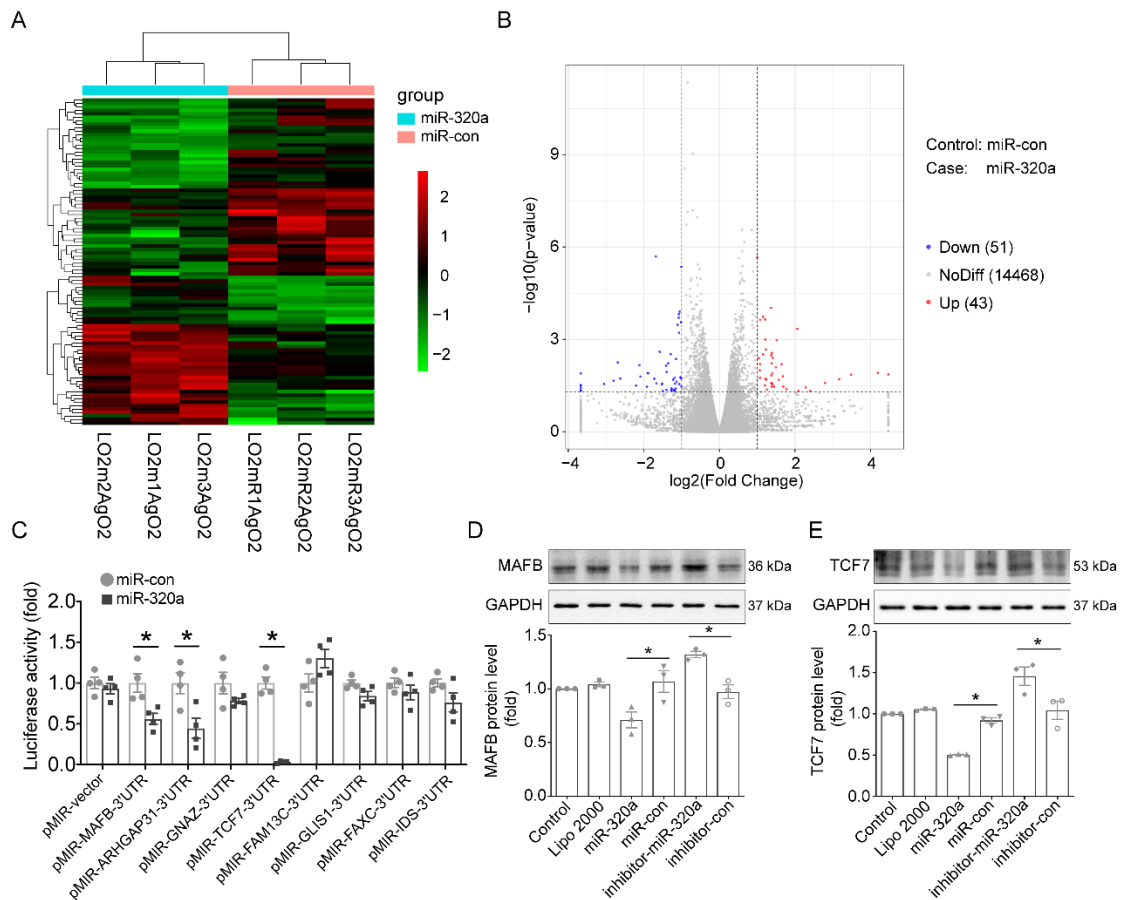
(A) The levels of circulating miR-320a in women with normal and high TG, normal and high TC as well as normal and high LDL-C (n = 163 for normal TG; n = 111 for high TG; n = 151 for normal TC; n = 123 for high TC; n = 187 for normal LDL-C; n = 87 for high LDL-C. Data are expressed as mean \pm SEM, Student's t test). (B) The correlation of circulating miR-320a levels with TG, TC or LDL-C (n = 274. The P values were produced by Pearson correlation analysis). (C) ORs (crude or adjusted for BMI) of HLP stratified by quartile level of circulating miR-320a (n = 274. Logistic regression with and without adjustment for BMI was used and data are expressed as ORs and their 95% CIs). Q1, first quartile; Q2, second quartile; Q3, third quartile; Q4, fourth quartile. TG indicates triglyceride; TC, total cholesterol; LDL-C, low density lipoprotein cholesterol; CI, confidence interval; OR, odds ratio.

Figure S3. Body and liver weight of mice with different treatments, Related to Figure 2.



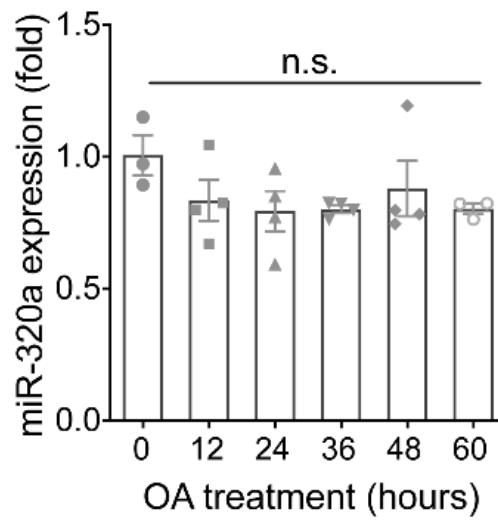
C57BL/6J mice were first injected with the corresponding rAAVs or normal saline in the caudal vein at 6 weeks of age. After 2 weeks, infected mice were subjected to normal diet or high-fat diet respectively for 4 weeks (n = 9-12). (A) Representative images of immunohistochemical staining using GFP antibody in different tissue sections of rAAV-TBG-GFP treated mice. Scale bar, 50 μ m. (B) Body weight of mice (n = 9-12). (C) Representative images of gross morphologies of livers. Scale bar, 50 mm. (D) Liver weight of mice (n = 9-11). Data are expressed as mean \pm SEM, *p < 0.05, Student's t test. ND indicates normal diet; HFD, high fat diet.

Figure S4. miR-320a targets TCF7 and MAFB, Related to Figure 3.



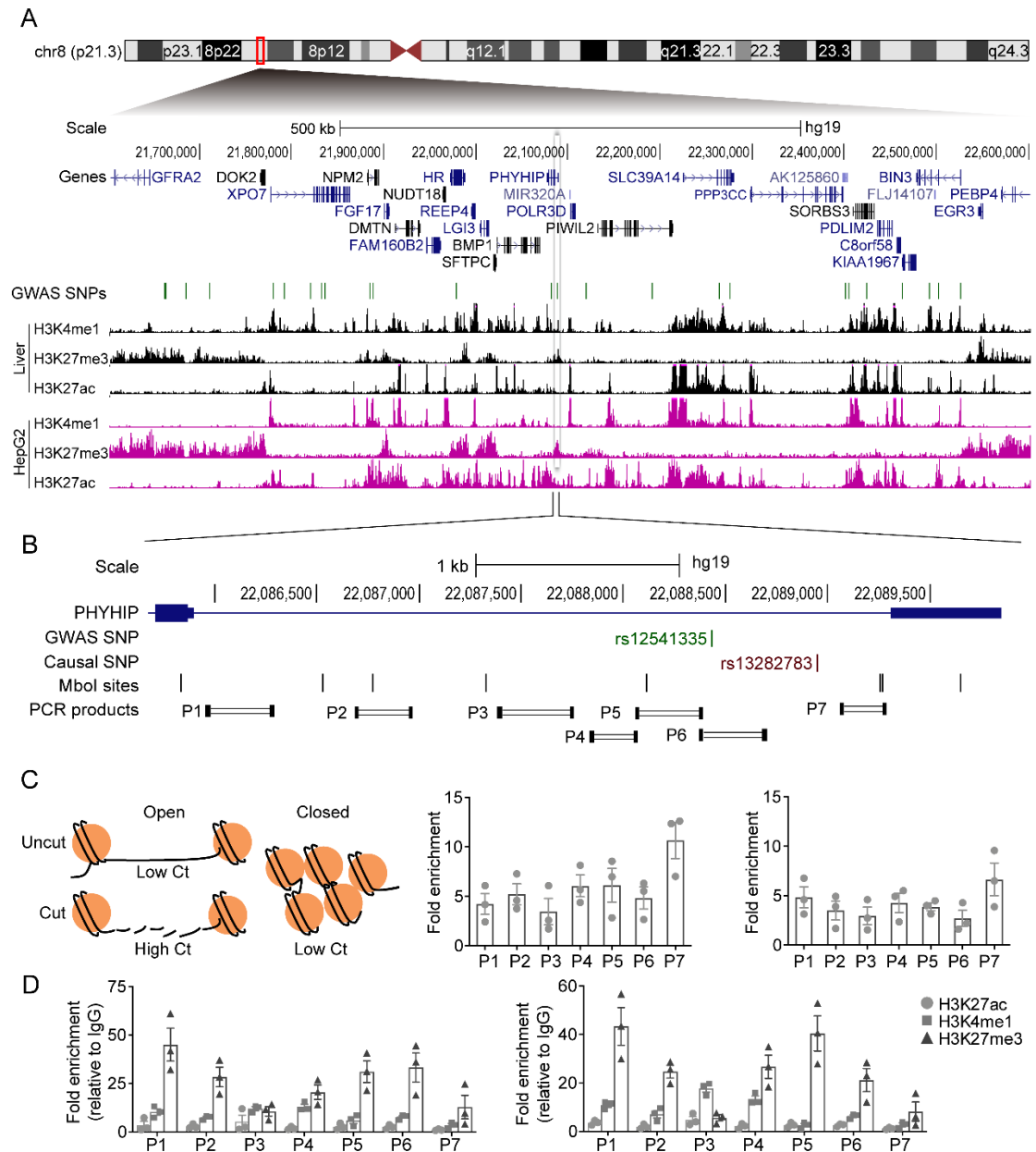
(A) Heatmap for 43 mRNAs identified by Ago2 RIP-seq showing increased association with the Ago2 protein after miR-320a transfection ($n = 3$ dishes per group). Hierarchical clustering analyses were performed based on all DEGs, and the miR-320a-transfected and miR-con-transfected groups were clustered. (B) Visualization of Ago2 RIP-Seq results with Volcano Plot. The red dots represent significantly upregulated genes, the blue dots represent significantly downregulated genes ($|\log_2 \text{FC}| \geq 1$ and $\text{FDR} < 0.01$), and the grey dots represent insignificant differentially expressed genes. (C) Regulation of putative targets mRNA via miR-320a targeting its 3' UTR was determined with luciferase reporter assays in HEK293T cells ($n = 4$ independent experiments). (D-E) L02 cells were transfected with miR-320a mimics/inhibitors (or their control). Representative Western blots and quantitative analysis of MAFB (D) and TCF7 (E) in L02 cells ($n = 3$ independent experiments per group). GAPDH was used as an internal control. For (C-E), data are expressed as mean \pm SEM, * $p < 0.05$, Student's t test.

Figure S5 miR-320a expression in OA treated cells with different time points, Related to the Figure 3.



L02 cells were subjected to 200 μ M oleic acid stimulation. Data are expressed as mean \pm SEM, n = 3-4 dishes per group, Student's t test.

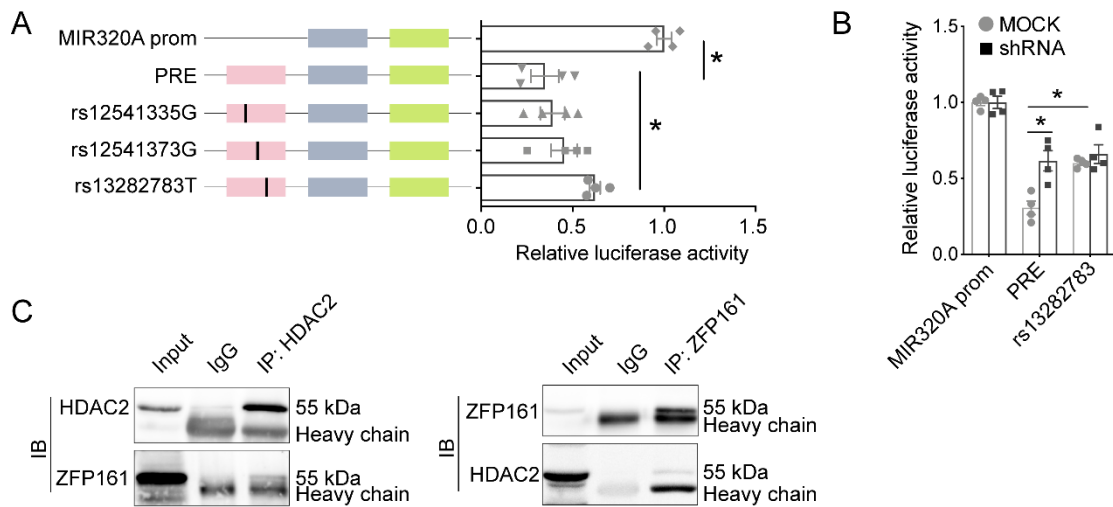
Figure S6. Functional characterization of rs12541335 association region, Related to Figure 4.



(A) GWAS identified significant SNPs with respect to their genomic landscape in a 1 Mb region around MIR320A. The image is based on the UCSC genome browser (human genome, version hg19; chromosome 8, nucleotides 21,602,475-22,602,556). The chromosome, scale and base position are shown at the top. The genes track shows the positions and structures of UCSC indicated genes which includes both protein-coding genes and non-coding RNA genes; gene structures are depicted with exons (vertical boxes) joined by introns (lines); the splice variants of each gene are not shown. The GWAS SNPs track displays the positions of SNPs (green ticks) identified by published GWAS, collected in the NHGRI-EBI GWAS Catalog published jointly by the National Human Genome Research Institute (NHGRI) and the European Bioinformatics Institute (EMBL-EBI). Tracks showing ChIP-seq data of histone marks

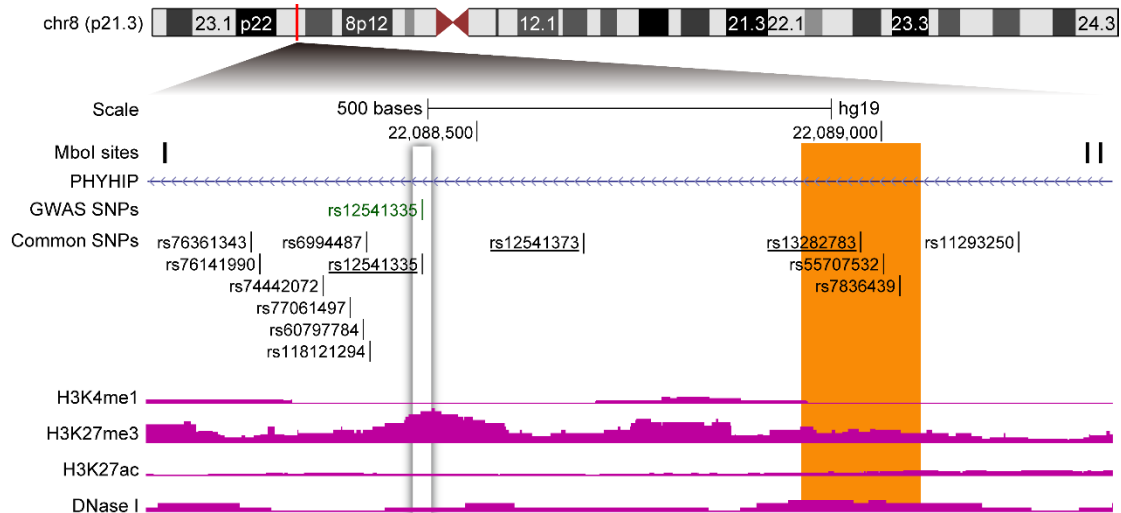
(H3K4me1, H3K27me3, and H3K27ac) in human liver tissue (black) and HepG2 cell line (purple) at the ENCODE portal are indicated at the bottom; the barplot of each track represent fold change over control. Inset box: GWAS identified rs12541335 overlaps the H3K27me3 peaks in both liver tissue and HepG2 cell line. GWAS indicates Genome-Wide Association Study; SNP, single nucleotide polymorphisms; H3K4me1, monomethylation of histone H3 Lys4; H3K27me3, trimethylation of histone H3 Lys27; H3K27ac, acetylation of histone H3 Lys27. (B) Zoomed-in view (chromosome 8, nucleotides 22,085,666-22,089,887) of the location of rs12541335 and nearby regions. The locations of PCR products using primers for CHART-PCR and histone marks ChIP-qPCR are shown at the bottom. PCR products are depicted by black bars (indicating primers) with parallel lines. (C) Chromatin accessibility assays using real time quantitative PCR (CHART-PCR) in L02 and HepG2 cells (n = 3 independent experiments). Schematic of the chromatin accessibility experiment is shown on the left. Chromatin was purified from L02 (medium) or HepG2 (right) and cut by Dnase. Chromatin accessibility at the region of interest was assessed by real time-PCR using primers shown in (B). Accessibility was calculated using the formula: enrichment = $2^{(Ct_{Cut}-Ct_{Uncut})}$. Ct indicates cycle threshold. (D) Histone marks chromatin immunoprecipitation assays using quantitative PCR (ChIP-qPCR) in L02 (left) and HepG2 (right) cells (n = 3 independent experiments). Chromatin immunoprecipitation assays were conducted with H3K27ac, H3K4me1 and H3K27me3 antibodies, followed by realtime-PCR using primers shown in (B). IgG was used to control for primer amplification efficiency and antibody specificity. ChIP-qPCR results presented as the ratio of sample/IgG. Formula: enrichment = $2^{-\Delta Ct}$, $\Delta Ct = (Ct_{sample}-Ct_{Input})-(Ct_{IgG}-Ct_{input})$. The sample means H3K27ac, H3K4me1 and H3K27me3, respectively. Data are expressed as mean \pm SEM, *p < 0.05, Student's t test.

Figure S7. Luciferase reporter assays and co-IP experiments in HepG2 cells, Related to Figure 5.



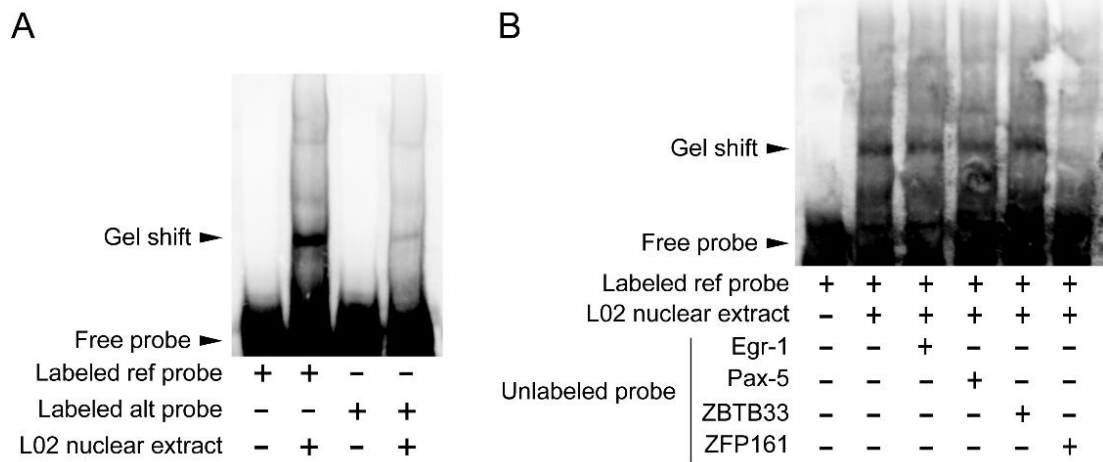
(A) Luciferase reporter assays following transient transfection in HepG2 cells. Alternative alleles (black bars) were engineered into the constructs which are denoted by corresponding SNP ID. (B) Luciferase reporter assays following transient transfection of corresponding constructs in HepG2 cells pre-treated with shRNA against ZFP161. (C) Immunoprecipitation with the anti-ZFP161 (left) or anti-HDAC2 antibody (right) in HepG2 cells, followed by Western blotting with antibodies for anti-ZFP161 and anti-HDAC2. For (A) and (B), data are expressed as mean \pm SEM, n = 4 independent experiments *p < 0.05, Student's t test.

Figure S8. Rs13282783 is located in one of distal DHSs which were highly correlated with MIR320A promoter DHS, Related to Figure 5.



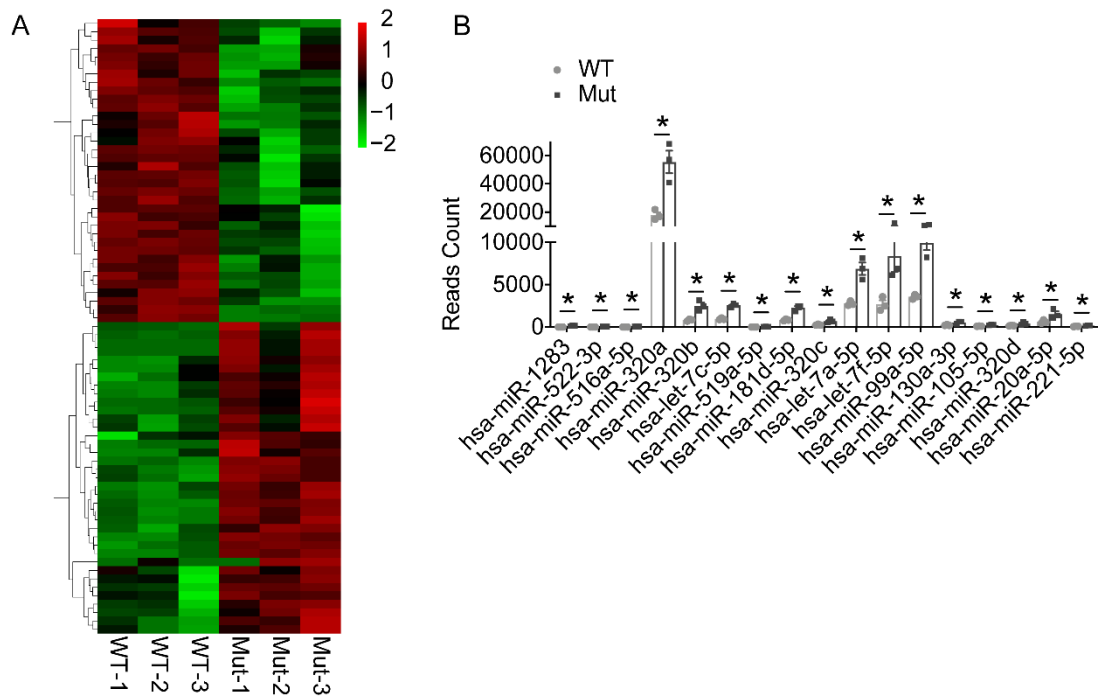
The genomic landscape of candidate causal SNPs. The image is based on the UCSC genome browser (human genome, version hg19; chromosome 8, nucleotides 22,088,106-22,089,268). The chromosome, scale and base position are shown at the top. Candidate causal SNPs locate in an intron of PHYHIP. The Common SNPs track displays the positions of SNPs (black ticks) with $\geq 1\%$ minor allele frequency, collected in the database dbSNP build 150. Tracks at the bottom show ChIP-seq data of histone marks (H3K4me1, H3K27me3, and H3K27ac) and in HepG2 cell line at the ENCODE portal; the barplot of each track represent fold change over control (ChIP-seq data) or read-depth normalized signal (Dnase I-seq data), which denotes that rs13282783 overlaps the DnaseI-seq peaks. The orange box (nucleotides 22,088,900-22,089,050) indicates one non-promotor Dnase hypersensitive sites (DHS) connected to MIR320a promoter DHS. GWAS indicates Genome-Wide Association Study; SNP, single nucleotide polymorphisms; H3K4me1, monomethylation of histone H3 Lys4; H3K27me3, trimethylation of histone H3 Lys27; H3K27ac, acetylation of histone H3 Lys27.

Figure S9. EMSA for candidate causal SNP rs13282783 to detect allele- predisposing binding of nuclear proteins, Related to Figure 5.



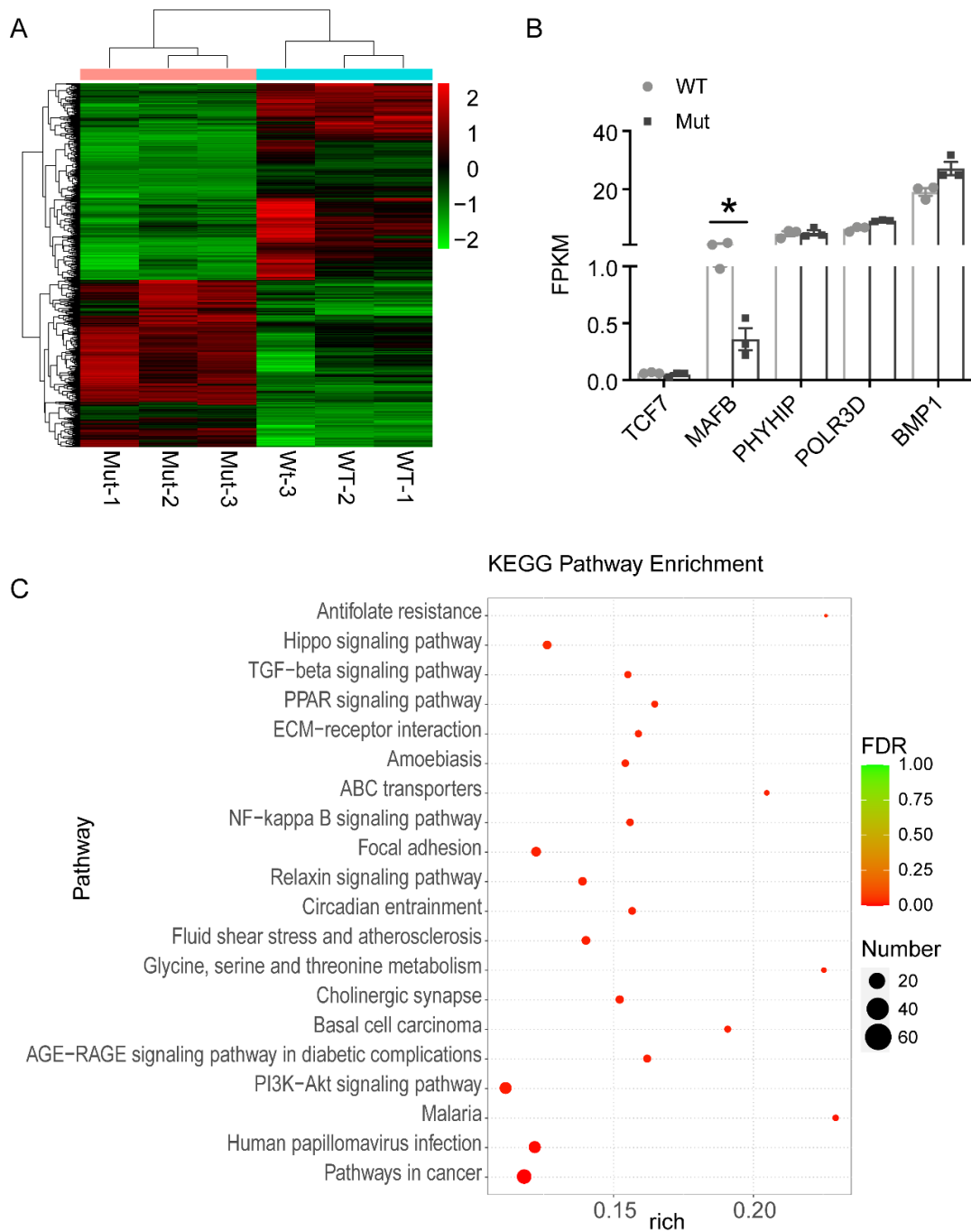
(A) Labeled probes for different alleles of rs13282783 were incubated with L02 nuclear extracts. The arrowheads indicate the gel-shift band of protein-DNA complexes. (B) Labeled probes for reference allele of rs13282783 and unlabeled probe for consensus binding site of different transcriptional factors were incubated with L02 nuclear extracts. Egr-1, Pax-5, ZBTB33 and ZFP161 indicates the oligonucleotides of their consensus binding site respectively.

Figure S10. miRNA-seq results in wildtype and mutant cells, Related to Figure 6.



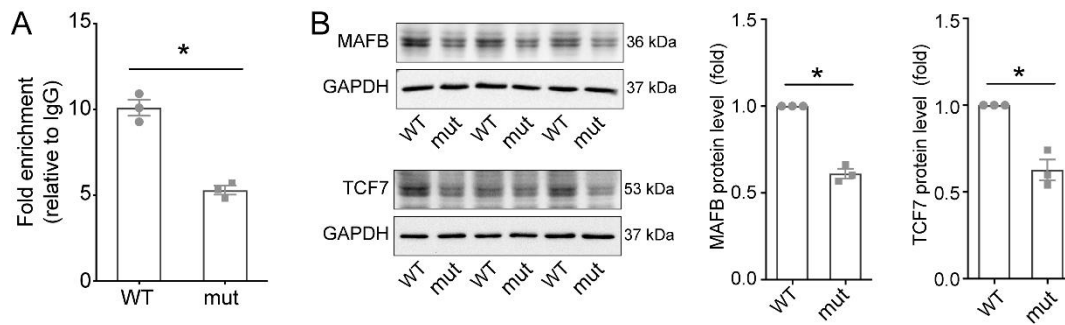
(A) Heatmap for differentially expressed miRNAs identified by miRNA-seq between wildtype and mutant cells (n = 3 dishes per group). Hierarchical clustering analyses were performed based on all differentially expressed miRNAs. (B) the expression of the up-regulated miRNAs (mutant L02 cells vs wildtype L02 cells). Data are expressed as mean \pm SEM, *means adjusted p-value < 0.05.

Figure S11. mRNA-seq results in wildtype and mutant cells, Related to Figure 6.



(A) Heatmap for differentially expressed mRNAs identified by mRNA-seq between wildtype and mutant cells (n = 3 dishes per group). Hierarchical clustering analyses were performed based on all differentially expressed mRNAs. (B) the expression of TCF7, MAFB, and the adjacent genes (PHYHIP, BMP1, POLR3D) of the causal SNP in mutant L02 cells and the wildtype cells. Data are expressed as mean \pm SEM, *means adjusted p-value < 0.05. (C) the results of the KEGG pathways enrichment analysis of the DEGs in mRNA-seq.

Figure S12. The effect of base editing of rs13282783 on ZFP161 binding and the protein level of MAFB and TCF7, Related to Figure 6.



(A) ChIP-qPCR on the region around rs13282783 in wildtype and mutant L02 cells (n = 3 independent experiments). (B) Representative Western blots and quantitative analysis of MAFB and TCF7 in wildtype and mutant L02 cells. GAPDH was used as an internal control. Data are expressed as mean \pm SEM, *p < 0.05.

Table S1. Correlation between plasma miR-320a level and anthropometric and metabolic parameters in men. (Related to Figure 1)

	unadjusted		Adjusted ^a		Adjusted ^b	
	r	p	r	p	r	p
Age	0.113	0.199	-	-	-	-
BMI	0.357	<0.001	0.341	<0.001	-	-
HDL-C	-0.176	0.045	-0.159	0.072	-0.049	0.587
LDL-C	0.357	<0.001	0.344	<0.001	0.234	0.008
TC	0.384	<0.001	0.373	<0.001	0.302	0.001
TG	0.518	<0.001	0.509	<0.001	0.446	<0.001
FBG	0.091	0.298	0.078	0.375	-0.025	0.782
2h-OGTT	0.090	0.302	0.068	0.442	0.002	0.985
HbA1c	0.175	0.045	0.160	0.068	0.060	0.501
SBP	0.133	0.127	0.103	0.242	0.029	0.745
DBP	0.040	0.647	0.044	0.618	-0.035	0.697

^aAdjusted for age; ^badjusted for age and BMI. BMI, body mass index; HDL-C, high-density lipoprotein cholesterol; LDL-C, low-density lipoprotein cholesterol; TG, triglycerides; FBG, fasting blood glucose; OGTT, oral glucose tolerance test; SBP, systolic blood pressure; DBP, diastolic blood pressure.

Table S2. Correlation between plasma miR-320a level and anthropometric and metabolic parameters. (Related to Figure 1)

	unadjusted		Adjusted ^a		Adjusted ^b	
	r	p	r	p	r	p
Age	0.082	0.101	-	-	-	-
BMI	0.236	<0.001	0.217	<0.001	-	-
HDL-C	-0.157	0.002	-0.142	0.004	-0.092	0.066
LDL-C	0.259	<0.001	0.242	<0.001	0.208	<0.001
TC	0.293	<0.001	0.277	<0.001	0.254	<0.001
TG	0.400	<0.001	0.390	<0.001	0.354	<0.001
FBG	0.084	0.093	0.076	0.130	0.027	0.585
2h-OGTT	0.107	0.032	0.089	0.075	0.047	0.348
HbA1c	0.153	0.002	0.139	0.005	0.079	0.115
SBP	0.123	0.013	0.092	0.066	0.073	0.144
DBP	0.040	0.426	0.036	0.472	0.018	0.713

^aAdjusted for gender and age; ^bAdjusted for gender, age and BMI. BMI, body mass index; HDL-C, high-density lipoprotein cholesterol; LDL-C, low-density lipoprotein cholesterol; TG, triglycerides; FBG, fasting blood glucose; OGTT, oral glucose tolerance test; SBP, systolic blood pressure; DBP, diastolic blood pressure.

Table S3. Correlation between plasma miR-320a level and anthropometric and metabolic parameters in women. (Related to Figure 1)

	unadjusted		Adjusted ^a		Adjusted ^b	
	r	p	r	p	r	p
Age	0.078	0.202	-	-	-	-
BMI	0.165	0.007	0.150	0.013	-	-
HDL-C	-0.145	0.017	-0.130	0.032	-0.103	0.091
LDL-C	0.208	0.001	0.194	0.001	0.181	0.003
TC	0.246	<0.001	0.234	<0.001	0.224	<0.001
TG	0.328	<0.001	0.321	<0.001	0.299	<0.001
FBG	0.082	0.176	0.074	0.222	0.046	0.453
2h-OGTT	0.113	0.063	0.100	0.101	0.071	0.243
HbA1c	0.141	0.020	0.128	0.035	0.089	0.146
SBP	0.115	0.058	0.089	0.146	0.083	0.173
DBP	0.045	0.463	0.035	0.570	0.032	0.605

^aAdjusted for age; ^badjusted for age and BMI. BMI, body mass index; HDL-C, high-density lipoprotein cholesterol; LDL-C, low-density lipoprotein cholesterol; TG, triglycerides; FBG, fasting blood glucose; OGTT, oral glucose tolerance test; SBP, systolic blood pressure; DBP, diastolic blood pressure.

Table S4. Candidate target genes of miR-320a identified by Ago2-RIP. (Related to Figure 3)

Genes	Description	miR-320a binding sites*	
		Human	Mouse
MAFB	MAF bZIP transcription factor B	+	+
ARHGAP31	Rho GTPase activating protein 31	+	+
GNAZ	G protein subunit alpha z	+	+
TCF7	transcription factor 7	+	+
FAM13C	family with sequence similarity 13 member C	+	+
GLIS1	GLIS family zinc finger 1	+	+
FAXC	failed axon connections homolog	+	+
IDS	iduronate 2-sulfatase	+	+
OLFML2B	olfactomedin like 2B	-	-
TUBB4A	tubulin beta 4A class IVa	-	-
IQCN	IQ motif containing N	-	-
CA11	carbonic anhydrase 11	-	-
PROC	protein C, inactivator of coagulation factors Va and VIIIa	-	-
IL22RA1	interleukin 22 receptor subunit alpha 1	-	-
VIT	vitron	-	-
MYO1A	myosin IA	-	-
C1orf116	chromosome 1 open reading frame 116	+	-
HSPA1L	heat shock protein family A (Hsp70) member 1 like	-	-
DTWD2	DTW domain containing 2	-	-
GJB5	gap junction protein beta 5	-	-
FGFBP3	fibroblast growth factor binding protein 3	-	-
SAT2	spermidine/spermine N1-acetyltransferase family member 2	-	-

FGB	fibrinogen beta chain	+	-
ZNF837	zinc finger protein 837	-	-
ZNF782	zinc finger protein 782	-	-
KIF12	kinesin family member 12	-	-
NIM1K	NIM1 serine/threonine protein kinase	-	-
TNC	tenascin C	-	-
TEK	TEK receptor tyrosine kinase	-	-
PRRX2	paired related homeobox 2	-	-
ELN	elastin	-	-
KBTBD4	kelch repeat and BTB domain containing 4	-	-
RIPK4	receptor interacting serine/threonine kinase 4	+	-
ZNF497	zinc finger protein 497	-	-
RFXAP	regulatory factor X associated protein	+	-
CCNI2	cyclin I family member 2	-	-
THAP8	THAP domain containing 8	-	-
DCN	decorin	-	-
IRF5	interferon regulatory factor 5	+	-
TNF	tumor necrosis factor	+	-
ROM1	retinal outer segment membrane protein 1	-	-
MORN3	MORN repeat containing 3	-	-
DNAAF3	dynein axonemal assembly factor 3	-	-

* miR-320a binding sites on 3' UTR of genes were predicted in the online computational tool, RNAhybrid, and a minimum free energy (MFE) of hybridization lower than -20 Kcal/mol was used as a cut-off setting.

Table S5. Summary of GWAS identified significant SNPs in a 1 Mb region around MIR320A. (Related to Figure 4)

SNP ID	Position	Trait or Disease	Function	Risk allele	Freq	P value	OR or Beta (95% CI)
rs76547188	chr8: 22120859	Obesity-related traits	Missense	A	0.01	5.00E-06	0.03 (NR)
rs3816788	chr8: 21974983	Lung cancer in ever smokers	intronic	A	0.44	3.00E-06	1.073 (1.042-1.1057)
rs2076940	chr8: 21978509	Mean corpuscular hemoglobin	intronic	A	NR	5.00E-07	0.0038 (0.0022-0.0054)
rs7833426	chr8: 21805336	Response to lithium treatment	intronic	A	0.92	2.00E-07	3.66 (2.37-4.94)
rs7843479	chr8: 21963302	Mean corpuscular volume	intronic	A	0.29	3.00E-08	0.072 (0.047-0.097)
rs7843479	chr8: 21963302	Mean corpuscular volume	intronic	NR	NR	1.00E-07	NR
rs58141407	chr8: 21934261	Red blood cell count	intronic	T	0.16	6.00E-15	0.038 (0.028-0.048)
rs58141407	chr8: 21934261	Mean corpuscular volume	intronic	T	0.16	4.00E-33	0.058 (0.049-0.067)
rs80207740	chr8: 21922426	Mean corpuscular hemoglobin	intronic	G	0.16	7.00E-33	0.058 (0.049-0.068)
rs202184555	chr8: 21827663	Blood protein levels	intergenic	GT	0.30	8.00E-16	0.22 (0.16-0.28)
rs2280104	chr8: 22668467	Parkinson's disease	intronic	T	0.37	3.00E-08	1.07 (1.04-1.09)
rs6558174	chr8: 22634616	Breast cancer	intronic	G	0.70	3.00E-06	0.036 (0.021-0.051)
rs7000551	chr8: 22418738	BNP to NT-BNP ratio	intronic	G	0.63	2.00E-09	0.109 (0.074-0.144)
rs11778693	chr8: 22605339	eye movement dysfunction	5' UTR	NR	NR	4.00E-06	1.25 (0.74-1.76)
rs11778693	chr8: 22605339	eye movement dysfunction	5' UTR	NR	NR	8.00E-06	1.95 (1.13-2.77)
rs7828089	chr8: 22406821	Verbal declarative memory	intronic	G	0.48	2.00E-06	NR
rs7828089	chr8: 22406821	Verbal declarative memory	intronic	G	0.48	2.00E-06	NR

rs12541335	chr8: 22230919	Hypertriglyceridemia	intronic	G	0.66	7.00E-06	1.23 (1.13-1.33)
rs12550716	chr8: 22031059	CSF biomarker levels	intronic	NR	NR	1.00E-16	NR
rs140244976	chr8: 22262244	Myringotomy	intronic	NR	NR	3.00E-07	2.5 (1.1-3.9)
rs2280890	chr8: 22547327	HIV-1 viral setpoint	intronic	NR	0.01	9.00E-06	NR
rs4075536	chr8: 22224195	Subjective well-being	exonic	A	0.80	3.00E-06	0.019 (0.011-0.027)
rs4242434	chr8: 22644317	eye movement dysfunction	intronic	NR	NR	8.00E-06	1.22 (0.7-1.73)
rs4872511	chr8: 22543476	HIV-1 viral setpoint	exonic	NR	0.01	9.00E-06	NR
rs11776272	chr8: 22027033	Obesity-related traits	intronic	G	0.18	5.00E-06	0.05 (NR)
rs13273616	chr8: 22333990	Takotsubo syndrome	intronic	C	0.53	6.00E-06	2.22 (NR)
rs17428041	chr8: 21853920	Neuropathic pain in T2D	intergenic	T	0.71	2.00E-07	1.49 (NR)
rs17581368	chr8: 21804933	Entorhinal cortical thickness	intronic	NR	NR	7.00E-06	NR

Data from the NHGRI-EBI GWAS Catalog published jointly by the National Human Genome Research Institute (NHGRI) and the European Bioinformatics Institute (EMBL-EBI). Chromosome position is based on human genome, version hg19. CI, confidence interval. Freq, frequency of the effect allele. GWAS, Genome-wide association study. OR, odds ratio. SNP, single-nucleotide polymorphism. UTR, untranslated region. CSF, cerebrospinal fluid. T2D, type 2 diabetes. NR, not reported.

Table S6. Summary of rs12541335 and linked SNPs in American LD ($r^2 \geq 0.2$). (Related to Figure 4)

SNP ID	position	LD	Ref	Alt	Number of motifs altered	Function	Located in the silencer element*
rs12541335	Chr8: 22088432	1	A	G	0	intronic	Y
rs12541373	Chr8: 22088632	0.64	A	G	1	intronic	Y
rs13282783	Chr8: 22088975	0.26	C	T	6	intronic	Y
rs7830106	Chr8: 22089383	0.21	C	A	8	5' UTR	N
rs11547658	Chr8: 22089477	0.25	G	A	5	5' UTR	N
rs62496063	Chr8: 22089764	0.22	G	A	1	5' UTR	N
rs3888282	Chr8: 22090263	0.25	T	G	3	intergenic	N
rs57413400	Chr8: 22091888	0.25	G	A	4	intergenic	N
rs6989830	Chr8: 22092121	0.21	T	A	38	intergenic	N
rs34354235	Chr8: 22092154	0.25	G	A	3	intergenic	N
rs6990334	Chr8: 22092426	0.21	T	G	0	intergenic	N
rs11774265	Chr8: 22092597	0.25	G	A	5	intergenic	N
rs7836017	Chr8: 22093323	0.21	G	C	7	intergenic	N
rs149036224	Chr8: 22094070	0.21	G	A	3	intergenic	N
rs7006381	Chr8: 22095294	0.21	T	C	0	intergenic	N
rs149674269	Chr8: 22097245	0.21	C	G	5	intergenic	N
rs116103252	Chr8: 22097482	0.21	G	A	11	intergenic	N

rs71513872	Chr8: 22097835	0.25	C	T	1	intergenic	N
rs199863565	Chr8: 22134545	0.29	TA	T	5	intronic	N
rs6995167	Chr8: 22134546	0.31	A	T	7	intronic	N
rs114463130	Chr8: 22134653	0.2	G	A	1	intronic	N
rs59163347	Chr8: 22137515	0.33	G	A	6	intronic	N
rs4871992	Chr8: 22146385	0.23	G	A	0	intronic	N
rs4872463	Chr8: 22147333	0.24	A	G	0	intronic	N
rs11779087	Chr8: 22148085	0.24	G	A	1	intronic	N
rs61115295	Chr8: 22152541	0.22	G	A	4	intronic	N
rs68063696	Chr8: 22153236	0.23	A	G	6	intronic	N
rs4872464	Chr8: 22153381	0.21	G	A	8	intronic	N
rs11985017	Chr8: 22153648	0.27	A	C	7	intronic	N
rs4565458	Chr8: 22154133	0.27	T	C	0	intronic	N
rs7834182	Chr8: 22163112	0.25	G	A	2	intronic	N
rs6993855	Chr8: 22163797	0.29	A	G	8	intronic	N
rs13257108	Chr8: 22165043	0.25	T	C	6	intronic	N
rs4266653	Chr8: 22169087	0.29	A	G	5	intronic	N
rs3923433	Chr8: 22169798	0.25	A	T	5	intronic	N
rs3923439	Chr8: 22170079	0.25	G	A	5	intronic	N

rs11135987	Chr8: 22173079	0.25	C	A	1	intronic	N
rs11135989	Chr8: 22175368	0.25	G	T	1	intronic	N
rs4872468	Chr8: 22179844	0.25	G	C	3	intronic	N
rs9792127	Chr8: 22180334	0.25	G	A	2	intronic	N
rs12542621	Chr8: 22184937	0.21	A	G	4	intronic	N
rs7012123	Chr8: 22196889	0.22	C	T	4	intronic	N
rs11135995	Chr8: 22200148	0.24	A	G	2	intronic	N
rs11779277	Chr8: 22200683	0.2	C	T	7	intronic	N
rs7003478	Chr8: 22201123	0.23	A	G	0	intronic	N
rs35068739	Chr8: 22201719	0.23	T	C	1	intronic	N
rs13252392	Chr8: 22204782	0.23	G	A	1	intronic	N
rs4871994	Chr8: 22206038	0.22	G	A	2	intronic	N
rs36028361	Chr8: 22206763	0.21	G	A	8	intronic	N
rs59283125	Chr8: 22212311	0.23	G	A	4	intronic	N
rs2290274	Chr8: 22214374	0.21	C	T	6	intergenic	N
rs11136002	Chr8: 22217082	0.22	C	T	2	intergenic	N
rs13261289	Chr8: 22219807	0.22	G	A	4	intergenic	N
rs34528906	Chr8: 22220033	0.21	A	G	2	intergenic	N
rs36105277	Chr8: 22220051	0.21	A	G	3	intergenic	N

Data from the HaploReg Tool. Chromosome position is based on human genome, version hg19. LD information from the 1000 Genomes Project. The effect of SNPs on regulatory motifs are predicted based on data of the Roadmap Epigenomics and ENCODE projects. LD, Linkage disequilibrium. SNP, single-nucleotide polymorphism. Ref, reference allele. Alt, alternative allele.

*whether is SNP located in the silencer element of MIR320A? Y indicates yes; N, no.

Table S7. Genomic coordinates of all distal, non-promoter DHSs within ± 500 kb correlated with MIR320A promoter DHS at threshold of $r > 0.7$ (Related to Figure 4)

CHR ID	Start position	End position	Correlation r
chr8	21608240	21608390	0.9158
chr8	21647600	21647750	0.84314
chr8	21674320	21674470	0.8025
chr8	21768160	21768310	0.78315
chr8	21769820	21769970	0.78102
chr8	21867780	21867930	0.86172
chr8	21894380	21894530	0.78295
chr8	21895120	21895270	0.82583
chr8	21899980	21900130	0.73384
chr8	21900640	21900790	0.73502
chr8	21905940	21906090	0.76791
chr8	21924380	21924530	0.85075
chr8	21965640	21965790	0.75237
chr8	21966600	21966750	0.78263
chr8	21969360	21969510	0.78479
chr8	22021620	22021770	0.71874
chr8	22035540	22035690	0.77604
chr8	22053940	22054090	0.70387
chr8	22058540	22058690	0.84595
chr8	22059180	22059330	0.79624
chr8	22063440	22063590	0.78884
chr8	22071380	22071530	0.87577
chr8	22077820	22077970	0.83146

chr8	22078900	22079050	0.80757
chr8	22088900	22089050	0.76629
chr8	22133220	22133370	0.81892
chr8	22149620	22149770	0.83439
chr8	22214120	22214270	0.80911
chr8	22217960	22218110	0.83793
chr8	22409520	22409670	0.75151
chr8	22419420	22419570	0.7186
chr8	22451320	22451470	0.79713
chr8	22476700	22476850	0.82744
chr8	22547700	22547850	0.7666

Data from *ENCODE Consortium Nature 2012* and *Thurman et al, Nature 2012*. Chromosome position is based on human genome, version hg19. DHS, DNase I hypersensitive site. CHR, chromosome.

Table S8. Regulatory motifs that rs13282783 may overlap. (Related to Figure 5)

PWM ID	Strand	Ref	Alt	Sequence of PWM
Egr-1_disc7	+	12.6	4.1	BGCGTGCC G YG
Gm397	+	7.3	12.4	DHNDTGTGCACAYAHDN
HDAC2_disc4	-	15.6	8.5	C G CGYDCGCG
Pax-5_disc5	+	14	10.5	GCGCSSG C GC
ZBTB33_disc2	+	11.7	9.8	SBSGCGR S VNS
Zfp161_3	-	12.2	8.8	HYRDRYGCG C GCSYHM

Data from the HaploReg Tool. In order to annotate SNPs by their effect on regulatory motifs, a library of PWMs was constructed from literature sources—TRANSFAC, JASPAR, and protein-binding microarray experiments (*Berger et al. 2006, Berger et al. 2008, Badis et al. 2009*). In addition, PWMs were discovered from ENCODE ChIP-seq experiments, resulting in a final library reported by *Kheradpour and Kellis. 2014*, which are denoted as disc_n. PWM, position weight matrix. The effect of reference (Ref) and alternate (Alt) alleles on regulatory motifs are shown as log-odds score in the third and fourth line, respectively. Abbreviation codes for degenerate bases: R, A/G; Y, C/T; M, A/C; K, G/T; S, G/C; W, A/T; H, A/T/C; B, G/T/C; V, G/A/C; D, G/A/T; N, A/T/C/G.

Table S9. Molecular characteristics of the human HCC cell lines. (Related to Figure 5)

Cell line	Gender	Age (yr)	Population	HBV DNA integration	Morphology	Other Molecular Characteristics
Hep3B	M	8	Negroid	+	Epithelial	mut. within FAS; p53 deleted
HepG2	M	15	Caucasian	-	Epithelial	Mut. in N-ras, β -catenin; p53 wt
L02	N.A.	Fetal	Asian	-	Epithelial	NA
SMMC-7721	M	50	Asian	-	Epithelial	p53 wt
Bel7402	M	53	Asian	-	Epithelial	NA
Huh7	M	57	Asian	-	Epithelial	K-ras wt; mut. in p53 (p.Y220C)
HLE	M	68	Asian	-	Epithelial	K-ras wt; mut. in p53 (p.G244A, p.R249S, p.V272M)
SNU-398	M	42	Asian	+	Epithelial	NA

HCC, hepatocellular carcinoma. M, male. wt, wild type; mut, mutation. +, positive; -, negative. NA, not available

Table S10. Baseline characteristics of the study sample for genotype. (Related to the Results)

	rs13282783			P value
	CC (n=834)	CT (n=1367)	TT (n=799)	
Age, yrs	59.26 ± 10.35	58.44 ± 10.34	58.60 ± 10.20	0.182
Male, %	43.30	45.40	46.20	0.463
BMI, kg/m ²	23.38± 3.35	23.20 ± 3.28	23.19 ± 2.96	0.364
SBP, mmHg	146.01 ± 23.89	146.92 ± 22.70	147.21 ± 23.34	0.545
DBP, mmHg	80.21 ± 12.22	81.28 ± 11.91	80.83 ± 12.56	0.139
TG, mmol/L	1.35 ± 0.83	1.48 ± 1.02	1.55 ± 1.13	<0.001
logTG	0.07 ± 0.21	0.11 ± 0.23	0.12 ± 0.24	<0.001
TC, mmol/L	4.93 ± 0.91	4.91 ± 0.93	5.01 ± 1.06	0.047
LDL, mmol/L	2.75 ± 0.76	2.74 ± 0.77	2.84 ± 0.84	0.014
HDL, mmol/L	1.49 ± 0.35	1.46 ± 0.36	1.45 ± 0.33	0.117
FBG, mmol/L	5.16 ± 0.41	5.15 ± 0.47	5.13 ± 0.42	0.573
2h-OGTT, mmol/L	6.04 ± 1.46	6.10 ± 1.39	5.99 ± 1.53	0.241
HbA1c, %	5.63 ± 0.39	5.60 ± 0.43	5.63 ± 0.43	0.121

BMI, body mass index; HDL-C, high-density lipoprotein cholesterol; LDL-C, low-density lipoprotein cholesterol; TG, triglycerides; FBG, fasting blood glucose; OGTT, oral glucose tolerance test; SBP, systolic blood pressure; DBP, diastolic blood pressure. Plus-minus values are means ± SD.

Table S11. Results of association between TG, TC, LDL and HDL levels and genotype of rs13282783 in the study sample. **(Related to the Results)**

	HDL			LDL			TC			TG		
	Standardized Effect Size			Standardized Effect Size			Standardized Effect Size			Standardized Effect Size		
	p	β^*	SE [†]									
rs13282783	0.150	-0.021	0.014	0.002	0.097	0.032	0.015	0.096	0.039	0.006	0.112	0.041

P-values were adjusted by linear regression for age, sex, BMI, hypertension, and diabetes. * β represents the proportion of 1 SD change in standardized trait values for each copy of the allele. † Standard error of β .

Table S12. Clinical characteristics of study samples for correlation between plasma miR-320a level and anthropometric and metabolic parameters. (Related to the Figure 1)

	study samples (N=404)
Age, yrs	55.01 ± 9.65
Male, %	31.9
BMI, kg/m ²	23.30 ± 2.61
HDL-C, mmol/L	1.49 ± 0.28
LDL-C, mmol/L	2.88 ± 0.90
TC, mmol/L	5.11 ± 1.12
TG, mmol/L, mmol/L	1.51 ± 0.88
FBG, mmol/L	5.42 ± 1.33
2h-OGTT, mmol/L	6.51 ± 2.94
HbA1c, %	5.70 ± 0.90
SBP, mmHg	139.85 ± 22.13
DBP, mmHg	78.25 ± 10.5

BMI, body mass index; HDL-C, high-density lipoprotein cholesterol; LDL-C, low-density lipoprotein cholesterol; TG, triglycerides; FBG, fasting blood glucose; OGTT, oral glucose tolerance test; SBP, systolic blood pressure; DBP, diastolic blood pressure. Plus-minus values are means ± SD.

Table S13. List of synthesized sequences and primers for luciferase reporter assays. (Related to Transparent Methods)

Name	Sequence (5'-3')
MAFB 3'UTR	GCTCTCAGCCCTGAGACACAGGCCTCAGTTAGGACGCTCGGCGCCCAAATCTCATCAGTTTTATTGCCTGCTCGATTATA TAGAAAAATACAAAAAATCTGCATTAATA
ARHGAP31 3'UTR	ACTAGTAAGATCTATTTTTATTTGGGGATAGACTGAGAAGCCACCATTTACATATTAACAAGTGACTTCAGTTCTAAGGGTTG AGATGCCTGTGTGGATTTATAAAATGGTTGCAAGATCTTTTAGACTCTGACATTTATAGCATCACCTTCAGGAACACAGTTC TGGGGATGTCATCATGAGACACACTGACAGCTGTGGAGATAGTCCCTACTCTCAGCTTTCCTTGCTAGTCAAGTCCAAAA GGCCTTAGAAGCTGACTCACCTTCTCAGCCAGAGTCCCTGCTGCTCAAGTGTGGACCTCCACTTTGACTCTCACCCAGCC TGCCAGCCATCACAAAGGCTTTCATAAACTTCCTGTGGTCTGGGCTAGCCTGGCACTGATGAAATTCCATTCTAAAGAAA GGCGGCCGC
GNAZ 3'UTR	ACTAGTGTGCAGGGTCTGTGCACCTTCCCTGCTGGCCTGCACACAGCTGCTCAGCACCACTTTTCATTCTGGACCTGGGA CCTTAGGAGCCGGGTGACAGCACTAACCAGACCTCCAGCCACTCACAGCTCTTTTTAAAAACAGCTTCAAATATGCAG CAAAAACCAATACAACAAAACGAGTGGCACGATTTATTTCAAACCTAGGCCAGCTGGGATTCCAGCTTTTCTTCTACTAGTC TGATGTTTTATAAATCAAAACCTGGTTTTCTTCTGACATTTTTTTTTTTGTTTTGTTTTTTGGTTTTTTTTTTTTTTGGCCA AATCTCGTGGTGTTCGCAGAAAAAATCCAGAAAATTTCAAATGCAGTTGAGTATTCTTTTTAAATGCAGATTTTCAAGC GGCCGC
TCF7 3'UTR	ACTAGTCCTGTAAACGTCATCTCAGGGTCCAGACCCTGAAGATTTTCAGAGGCTGCAGGACTTCTGCCTGAACCTGGGGT CATCGATTCAAACCTGCTCCAAGTGGTGGGAATCAGATCTGTCTTGATGTGTCATCTAATTAAGGGAATCCCTTGACCTATG GCTGCCTGCATCTATTCTTTGTACCATCTGTCTTGCCAGCCAGAAGCCTCTGCCTCCCTAGCTTTTCTGCTATAGGTCAGA GATGGGCTGAACTGAGCCTAGCTACCTTCTTACCCATCTCCCCATCCCCACTGCCACACCCTCCCCATTCCAGACACT TCATGGACCAAGAATGAGCTGGTTTGTCAAACAACATGTGAGCATGGTCAACAAGCACAAAGCTCAAGATGACAGCTCTTC TAAGCGGCCGC
FAM13C 3'UTR	ACTAGTAGTTTTTTAAACAAACAGGAAGAAGTCCACAAAAGGAAGATAGGATACCAATGGCAGATGAGTATTATGAATATAA GCACATAAAAGCCAAACTGAGACTATTAGAGGTCTCATCAGCAAGCAAGATGTGGCCAAAACCTATTTGAGGTTTCAGGAA ATGTTATGATCACTTTTACCCATGATATAAAGTAAAGTTTATTTTCTCTGCCATCCTTGCTAAGTAGTTTTGACACAATGAAA ATGGAAGCACTTTAGTGGTAGTATTAGCTGTTTTTAAGAAGGAATAGCAAGTTTAATTATATACAAGGAGAAGGGATTTAAAC

	GGGGGAAGAATACAACAGGTAGCCATATAATTGGGAAAAAATTCAGTGTCTCCATGCCAAGCAGAAAACATAGCGG CCGC
GLIS1 3'UTR	ACTAGTCATCTACACAGACACCTGAAGGAGCCCCACATGCGCCTGCCATCCAGCACTGCAGATGCCACCTCGCCCAC CTGCTGTCGCTCCCACCCTCCGTGCACCTAGCAGGAGTGCCAGGCCACAGCCGGAACAGCCAGGCCATGACCCAGGG GAGCCAGCGCTGCCACCCACCCAGCGCTGCCAGGGAGCCGCCATCCGAGCTTGAGCTGGGCGCACAGAGGTGCC GCCAGGATCTGTGGCCCTGTAACATTCCCTCGATCTTGTCTTCCCGTTCCTCCCCGCAGTGGTTTTGAAATCACAGACCT CGTGTATATAAAATATGCAGAACTTGTTTTCCGTTCCCCTGCCAGTTTTATATTTTTGGTTTTACAAGAAAAACATTA AAAAC TGAAAGGAGCGGCCGC
IDS 3'UTR	ACTAGTCAAGAGGGCTCCCCTGCCAATGAGGAACAAAAGCTCAAGGTCTAGTAGTGTATTGAGCACATGCTAGGAAACA AGAGTTGGGACGTGGACAAGGAGAGGAGCAAAGGCCAGGGGTAACTGCTTTTGGTTTTTCTCTATAAAAGTCAGGGA CTATGATTTATATGGGTGAGAAGGTTTGGAGTAGGACTGAAGCTGCCATTTACAAACCCCTTGCCCTAATTTATTGTAGTTT TGGGTGTGTTTCTGAAAGAACCCTTTCAGAGTGATTTTTATTGAGTACTCATTAACTTACAGCTTTTATGAATTCACATCTTC TACACTATTGAAAAACATAAGTTTGTATTGTGTTAAGTGCAGCATGAGTTATTATATGAATAAATCACATTAATTTGCCAGCG GCCGC
FAXC 3'UTR	ACTAGTGAAATGATCCAATGTCCGTTTCCTTTGAGTGTCATGTTAGTGCTCAAAAAGTTTTGGATTTTGGAGCGTTTCAGAT TTTGGATTTTGGATTTGGGATGCTCGACCTGTAGTTTGGTTTTTCATCTTTTACTCCATTTCTTTGACCTATAAATCCT ATCAGCCCTGTTTATTAACATAGACCCTAGTCAGAAATACTTTGAAATAGATCTACATCTACTTCAACGTCAGTTGGTTCCAC ACCCTTCTAGAACTTGTGTGGGGTCCTGGACTTCCCGTCTGTCCTGTTAGGGAAGCTTTGCTGTCCTAGCTTTCAGGACT CATCAGAGGGAAGAGGGTCATTTACCTTTCCAATGTGCTGTGATCTCAGAGTCGTTAAAATACATGTTTTGCTGCCAGCGG CCGC
h-MIR320A promoter-F	CTCTGCCCTTCAACCACCT
h-MIR320A promoter-R	ACCCAGCTTTTCCCGACTC
PRE-F	TTGAGGCAACACCCGAGAA
PRE-R	CCAGTGGAGCCAGGTGAGTA

F, forward primer; R, reverse primer; PRE, putative regulatory element.

Table S14. List of primers for Chromatin Conformation Capture assay. (Related to Transparent Methods)

Primer (Mbo I)	Sequence (5'-3')
Bait	CCGACTCTTAAGTCCAGGTCTCA
Fragment 1	CTGAACTGTACACTTCAAATGGTC
Fragment 2	CTGAGAAACAGGGTACAAACAGAGA
Fragment 3	GAAGGGAAAATATGCCTTATTCTTT
Fragment 4	CTTGTTGGAATTCTTATTCTCCTTC
Fragment 5	GTACATGGCTGGAAGGACAAGT
Fragment 6	TTCTAAATGTCACCTCCTTCTCTTC
Fragment 7	CAAGTTCTCTACACCCAGAAGACTG
Fragment 8 (PRE)	AGAGACTGGATTGAGCCATTAACC
Fragment 9	GAGAGGCAAGAGCGAAATCAAA
Fragment 10	AGCTGGGGTGGCTGTCTTCAG
Fragment 11	AAGAACATCCAAGGAAATGTGAGTC
Fragment 12	CGAGCTGGTGAGCTCAGAAGA
Fragment 13	CTCGCTCTGTTGTTCTGTCTCC
Fragment 14	GACAACCTATAACCTTCACTGGTCA
Fragment 15	GCCATTGGGAAGTTTAGAGCA
Fragment 16	TTTGGATGGGCACATAGGTTT
Fragment 17	GGTGTGGAATAGGCAGAGACACA
Fragment 18	GGACTGTAAGTGCACACGACCA
Fragment 19	CAGGAGTGAAGGAGGATTGAAGA
Fragment 20	GGTGGTTCTCATCACTGTCTCTG
Fragment 21	CTTCAAAAACCTTTGGGTTTCAGAG
Fragment 22	TTCAATCTTCTGTTTTCTGACCCTT
Fragment 23	AGGCTTGACACTTTTCTAACTACA

Fragment 24
Fragment 25
Fragment 26
Fragment 27
Fragment 28
Fragment 29
Fragment 30
Fragment 31
Fragment 32
Fragment 33
Fragment 34

GATTTTCTGTTTCCGAGGTTAGG
TGCTCATGTATATTATTTAGCCTC
GCAGCAAGTAGGGTAGGTCTCC
TTCCAATGAAAGCACGACC
GCAGTGCTAAGGTTTGGATGTTT
CGTACTCATTCAATACAAAGACCAC
CCCACTACCACATCTTGAGTCTG
CCTGCTCCTCCCTGAGACAA
AGTCTCACCCCTATCACCCATC
TTCAGGCAGTTCTCATGTCTCAG
TTCAGGCAGTTCTCATGTCTCAG

Table S15. List of primers of real time PCR for P1-P7 functional characterization, anti-HDAC2/ZFP161 ChIP around rs13282783 and anti-Ago2 co-IP in human LRP6 mRNA 3'UTR. **(Related to Transparent Methods)**

Primer (Mbo I)	Sequence (5'-3')
P1-F	CACCTATTCCTGCCTCTCCTTGG
P1-R	TCCCTCACACCCTGCCCTTC
P2-F	GTCCTCCTCCCAATATCCCTTTTCG
P2-R	CGTTTCCTCCGCCTCTCACC
P3-F	ACAGATGAGGCGACTGAGGTTG
P3-R	TGGACGAGCAGCAGACATAAGG
P4-F	TAACTGTGAGTTGCCTGGATGG
P4-R	TTGGGTAGGAGTGTGTCTGTGTTC
P5-F	CAGGGTGTGAGGGACAGGTTG
P5-R	GAGGCGGTGTGCGTGGAC
P6-F	ACGCACACCGCCTCACAAG
P6-R	GAGCAGGATGGAGTGGGTAAAGAG
P7-F	CCACCCTGCTGTCCCTGTTG
P7-R	ACCTGCTGCTGTTGATCCTGAG
rs13282783-F	CACACCCACAGGCTACTCAAATAAG
rs13282783-R	AGCGATGCCAACAGGGACAG
h-LRP6-F	CTATTCTCATCACCTCTACC CACC
h-LRP6-R	CCTTTATTATTCCTGTTTCCTTTGT

Table S16. Sequences of oligonucleotides used in EMSAs. (Related to Transparent Methods)

SNP	allele	Sequence (5'-3')
rs12541335	Ref	GCCACAGGCACCAACATGC A TGTGTGCCACCTCCACAAG
	Alt	GCCACAGGCACCAACATGC G TGTGTGCCACCTCCACAAG
rs12541373	Ref	CATGCCAACAGGTTTGTGC A CCTACGTGGCTCTGCCCAC
	Alt	CATGCCAACAGGTTTGTGC G CCTACGTGGCTCTGCCCAC
rs13282783	Ref	TCCAGCCAACTCGCGAGCG C GCACACACACACGCCGCGC
	Alt	TCCAGCCAACTCGCGAGCG T GCACACACACACGCCGCGC

Ref, reference; Alt, alternate.

Transparent Methods

Ethical Statement

This population-based study was designed in accordance with the Declaration of Helsinki and approved by the Ethics Committee of Tongji Hospital, Tongji medical college, Huazhong University of Science and Technology (HUST). Animal study was approved by Institutional Animal Care and Use Committee of Tongji Medical College of HUST and complied with the Guide for the Care and Use of Laboratory Animals standards (National Institutes of Health publication No. 86-23, revised 1985).

Subjects study

The written informed consent in population-based study was given by all subjects before participating in the study. The subjects were enrolled from the general population of Chinese Han descendant as described elsewhere (Cui et al., 2014). Medical histories of all participants were assessed via standardized questionnaires. There was no use of medications, alcohol or drug abuse, thyroid dysfunction and current pregnancy among members. Anthropometric parameters (height, weight and waist circumference) were measured and the body mass index (BMI) was calculated. Blood pressure and heart rate were measured and blood samples were collected via median cubital veins after overnight fast. Whole blood was collected into EDTA-anticoagulant vacutainers and immediately separated into plasma and cellular fractions by centrifugation. Total cholesterol (TC), low density lipoprotein-cholesterol (LDL-C), high density lipoprotein-cholesterol (HDL-C) and TG levels in blood samples were quantified on the Roche modular DPP system at the Department of Clinical Chemistry, Tongji Hospital. Hyperlipidemia was defined as a TC level of higher than 5.18 mmol per liter, or a LDL-C level of higher than 3.37 mmol per liter, or a HDL-C level of lower than 1.04 mmol per liter, or a TG level of higher than 1.7 mmol per liter (Jellinger et al., 2012). The plasma miR-320a levels were determined in 172 subjects with hyperlipidemia and 232 matched controls and their clinical characteristics are shown in Table S12. Another population, total of 3000 subjects, furthermore, were recruited for genotyping and their clinical characteristics are shown in Table S10.

Clinical characteristic data of human subjects were expressed as means \pm SD. The levels of circulating miR-320a in men were expressed as means \pm SEM and compared between normal and high TG, normal and high TC as well as normal and high LDL-C by Student's t tests. The unadjusted correlation between circulating miR-320a level and metabolic parameters was evaluated by Pearson's correlation coefficients. Adjusted correlation coefficients were derived from partial r^2 values obtained from analysis of covariance models that included each of the metabolic parameters. The associations between the quartiles of circulating miR-320a level and risk of hyperlipidemia (or high TC, high TG, high LDL-C) were determined by logistic regression with and without adjustment for BMI and expressed as odds ratio (OR) and their 95% confidence interval (CI). To test association between the SNPs and metabolic parameters, multivariate linear regression analyses were performed based on the dominant genetic model

after adjusting for gender and age with the Bonferroni correction method.

Reagents

Cell culture medium, DMEM and OPTI-MEM, and fetal bovine serum (FBS) were purchased from GIBCO (Thermo Fisher Scientific, Waltham, MA). The reverse transcriptional and real-time PCR primers of miR-320a, U6 and cel-miR-39-3p, mimics of cel-miR-39-3p, mimics and inhibitors of miR-320a and negative controls were from RiboBio (Guangzhou, China). Lipofectamine 2000, Trizol, Trizol LS were from Invitrogen (Thermo Fisher Scientific, Waltham, MA). The primers of mRNA real-time PCR were designed and synthesized by BGI (Shenzhen, China). The antibody against TCF7 was from Proteintech Group, Inc (Rosemont, IL). The antibodies against MAFB and TCF7 were from Cell Signaling Tech (Danvers, MA), and antibodies against H3K4me1, H3K27me3, H3K27ac, HDAC2 (for IP and Western blotting) were from ABclonal Biotech (Cambridge, MA). Anti-ZFP161 antibodies was from Santa Cruz Biotech (Dallas, TX). Antibodies against HDAC2 for ChIP was from Abcam (Cambridge, MA). Polyvinylidene difluoride membranes were from Millipore (Merck KGaA, Darmstadt, Germany). The Protein A/G Magnetic Beads, horseradish peroxidase-conjugated secondary antibody and ECL system were from Pierce Biotech (Thermo Fisher Scientific, Waltham, MA). Restriction enzymes of Mbol, HindIII, KpnI, MluI, SpeI, BamHI, BglII, T4 DNA Ligase and corresponding reaction buffer were from New England Biolabs (Ipswich, MA). Other reagents were from Sigma-Aldrich (Merck, St. Louis, MO) unless specified description elsewhere.

RNA immunoprecipitation sequencing (RIP-seq)

L02 cells were lysed and then incubated with anti-Ago2 antibody (Abnova Corporation, Taiwan, China) after transfected with miR-320a mimics or miR-con for 24 h. After incubating at 4 °C overnight, protein A/G magnetic beads (Thermo Scientific, Shanghai, China) were added into the solution and incubated for another 2 h at 4 °C. Then, the beads were washed five times with PBST and the remaining products were extracted with TRizol agent. RIP-seq assays and analysis were conducted by personalbio (Shanghai, China).

Luciferase reporter assay

To evaluate the direct binding of miR-320a and the target mRNA, pMIR-REPORT luciferase vector was employed. The sequence containing predicted miR-320a binding sites of the human mRNA 3' UTR were synthesized and inserted into pMIR vector. miR-320a mimics or negative controls were co-transfected with appropriate pMIR construct into HEK293T cells using Lipofectamine 2000.

To evaluate the activity of the promotor and the putative regulatory element, pGL3 vector was employed. The promotor of has-miR-320a has been identified by previous study and was amplified from human genomic DNA by PCR with specific primers. The reporter constructs driven by miR-320a promoter was generated by inserting the PCR products into the KpnI and BglII sites upstream of the firefly luciferase gene of pGL3-Basic vector (Promega, Beijing,

China). The putative regulatory element (PRE) identified by bioinformatic and functional analysis was amplified and inserted into the BglIII and HindIII sites upstream of the miR-320a promoter of pGL3 constructs. The alternate alleles of candidate causal SNPs were introduced into the PRE sequences by site-directed mutagenesis with the kit of Takara (Takara Biomedical Tech. Beijing, China). The luciferase constructs were transfected into immortalized human hepatic cell lines—L02 and HepG2 in 24-well plates under routine conditions. For silencing, cells were pre-treated with shRNA against ZFP161 or negative control and transfected with the relevant luciferase reporter plasmids. The pRL-TK plasmid carrying the Renilla luciferase gene was co-transfected as an exogenous control to normalize the cell number and transfection efficiency. Forty-eight hours after transfection, cells were harvested and incubated with passive lysis buffer. Luciferase activity of individual cell lysate was detected using the Dual Luciferase Reporter Assay System according to the manufacturer's instruction. List of synthesized sequences and primers for luciferase reporter assays are shown in Table S13.

Chromatin conformation capture assay

Chromatin Conformation Capture (3C) technology was employed in HepG2 and L02 cells as previously described (Painter et al., 2016). Ligation products were analyzed by real time qPCR using primers designed within restriction fragments (Table S14). Real time qPCR was performed on a Life Technologies 7900HT FAST Real-Time PCR System (Thermo Fisher Scientific, Waltham, MA) with SYBR rapid quantitative PCR Kit. A single Bacterial Artificial Chromosome (BAC) clone covering the genome segment flanking MIR320A was (Invitrogen, Cat# 6059757, Thermo Fisher Scientific, Waltham, MA) used as qPCR control template to normalize the amplification efficiency of different primers. 3C-qPCR data are normalized toward the signal of the BAC clone and GAPDH.

Chromatin accessibility assay

Chromatin accessibility assays were performed in HepG2 and L02 cells with an EpiQuik kit according to the manufacturer protocols (EpiQuik, Farmingdale, NY). Briefly, chromatin was immediately isolated after cell lysis and split in two. The one was cut with nuclease (Nse) mix, and the other as uncut control. DNA was purified after Nse digestion and amplified by real-time qPCR using primers specific for the location of rs12541335 and nearby regions (Figure 4B, Table S15). Accessibility was calculated as fold enrichment (FE) using the formula: $FE = 2^{(Ct_{Cut} - Ct_{Uncut})}$ (Rendeiro et al., 2016).

Chromatin immunoprecipitation assay

Chromatin immunoprecipitation (ChIP) assays were performed in HepG2, Hep3B, L02 cells with the ChIP Assay Kit (Beyotime, Shanghai, China) according to the manufacturer's instruction. In brief, cells were fixed by formaldehyde of 1% final concentration to crosslink protein and genomic DNA. After quenching formaldehyde with glycine, cells were lysed by sonication in SDS lysis buffer supplemented with a protease inhibitor PMSF. After

centrifugation, the supernatant was precleared with Pierce Protein A/G Magnetic Beads and subjected to immunoprecipitation with antibodies for anti-H3K4me1, anti-H3K27ac, anti-H3K27me3, anti-HDAC2 or anti-ZFP161, and negative control IgG. The antibody-protein-DNA complex was pulled down using Pierce Protein A/G Magnetic, eluted in elution buffer, and de-crosslinked. The DNA fragments enriched in ChIP assays were extracted with QIAquick PCR Purification Kit (Hilden, Germany) and quantified by real-time qPCR. Primers for qPCR are listed in Table S15. ChIP-qPCR results presented as the ratio of sample/IgG [enrichment = $2^{-\Delta\Delta Ct}$, $\Delta\Delta Ct = (Ct_{\text{Sample}} - Ct_{\text{Input}}) - (Ct_{\text{IgG}} - Ct_{\text{Input}})$]. The sample means H3K27ac, H3K4me1 and H3K27me3, respectively.

Electrophoretic mobility shift assay

Electrophoretic mobility shift assays (EMSA) were performed with the LightShift Chemiluminescent EMSA Kit according to the manufacture's instruction (Thermo Fisher Scientific, Waltham, MA). L02 nuclear protein extracts and biotin-labeled DNA duplexes were employed. Nuclear protein extracts prepared from L02 cells using the NE-PER Nuclear and Cytoplasmic Extraction Kit (Thermo Fisher Scientific, Waltham, MA). The concentrations of nuclear protein extracts were determined by Bradford's method. The probes carrying the sequence flanking candidate causal SNPs were prepared by annealing the oligonucleotides and their complimentary strands (BGI, Shenzhen, China). Labeled probes were biotinylated at the in 5' end of oligonucleotides in advance. Binding reactions were performed by incubating the labeled probes for different alleles of candidate SNPs with L02 nuclear extracts. DNA-protein complexes were separated on 6% native polyacrylamide gels by electrophoresis, transferred to positively charged nylon membrane, cross-linked under UV lamp, and visualized by ECL system. For competitive binding tests, unlabeled probes were used at 100-fold molar excess as competitor of labeled probes under the same condition. For the supershift assay, anti-ZFP161 antibody was added to the nuclear protein extracts and then maintained on ice for 20 min before the incubation of probe. Sequence of oligonucleotides are listed in Table S16.

Cell culture and treatments

L02, HepG2 and HEK293T cells were from American Type Culture Collection (ATCC, Manassas, VA) were cultured in DMEM medium supplemented with 10% FBS. L02 cells were transfected with miRNA mimics/inhibitor (100 nM) using Lipofectamine 2000 according to manufacturer's description, respectively, and then subjected to 200 μM oleic acid-bovine serum albumin complex (molar ratio 4:1).

Co-immunoprecipitation assay

Lysed extracts of HepG2 and L02 cells were immunoprecipitated with antibodies for anti-ZFP161 or anti-HDAC2. After incubating the primary antibodies into the cellular lysed extract overnight, Pierce Protein A/G Magnetic Beads were added. Next, the beads were washed and resuspended in Laemmli buffer. The immunoprecipitated samples were subjected to Western

blotting using corresponding primary antibodies and a conformation-specific secondary antibody that only recognizes native IgG (Cell Signaling Technology, Beverly, MA).

Genome editing using the VRER-BE3 system

pBK-VRER-BE3 was a gift from David Liu (Addgene plasmid Cat# 85173)(Kim et al., 2017). To generate of mutant L02 cells with a homozygous risk genotype (TT) at rs13282783, sgRNA recognizing chr8: 22,088,970-22,088,989 (hg19) was designed according to NGCG PAM of VRER-BE3. U6 promotor driven gRNA and hPGK promotor driven puromycin resistance gene was inserted into pBK-VRER-BE3 vector. At ~70% confluence, pBK-VRER-BE3-u6-gRNA-hPGK-Puro was transfected into L02 cells using Lipofectamine 2000 according to manufacturer's description. Puromycin was used for selection of L02 cells with plasmid integration. Then, cells resistant to puromycin were expanded for 5–7 days to form distinct colonies derived from single cells. Genomic DNA of each colony was extracted and the region containing rs13282783 was PCR amplified. Sanger sequencing was subsequently performed to identify that the mutation was successfully introduced. Sequences of sgRNA is showed in Figure 6A.

Western blotting

Total protein was obtained from cell or tissue lysates and simultaneously underwent protein denaturation. Next, the protein samples were separated by SDS-PAGE electrophoresis and then transferred to PVDF membranes. After incubation with specific primary antibodies and peroxidase-conjugated secondary antibodies, visualization of the target bands was allowed by enhanced chemiluminescence (ECL) system according to the manufacturer's instructions (Thermo Fisher Scientific, Waltham, MA). The intensities of target bands were analyzed by densitometry using Image J program (NIH).

RNA isolation and real-time PCR

Total RNA was isolated from cells and tissues with TRIzol Reagent. Plasma was incubated with exogenous control cel-miR-39-3p mimics and followed by RNA isolation with the TRIzol LS Reagent. Total RNA was reverse-transcribed by RevertAid First Strand cDNA Synthesis Kit (Thermo Fisher Scientific, Waltham, MA). Real-time PCR assays were performed with SYBR rapid quantitative PCR Kit according to the manufacture's instruction (Kapa Biosystems, Woburn, MA) on a Life Technologies 7900HT FAST Real-Time PCR System (Thermo Fisher Scientific, Waltham, MA). The relative miRNA levels were determined after normalizing to the level of internal control U6 or exogenous control cel-miR-39-3p. The relative mRNA levels were determined after normalizing to GAPDH level.

Animal study

To manipulate the hepatic expression of miR-320-3p in mice, the recombinant adeno-associated virus (rAAV, type 8) system with liver-specific promoter (thyroxine-binding globulin,

TBG) was employed. The rAAV system was a kind gift from Dr. Xiao Xiao (University of North Carolina Eshelman School of Pharmacy, Chapel Hill, NC). The anti-miR-320a-3p sponge and miR-320-3p were synthesized as precisely described (Yin et al., 2016) and cloned into pAAV8-TBG-eGFP vector, which was verified by sequencing. Oligonucleotides were synthesized and cloned into plasmid, respectively. rAAVs were packaged via triple plasmids co-transfection in HEK293 cells and purified as described previously (Yin et al., 2016).

Six-week-old male C57BL/6 mice were obtained from the Experimental Animal Center of Changsha (Changsha, China) and maintained in a temperature-controlled and specific pathogen-free barrier facility with a 12-h light/dark cycle in Laboratory Animal Center of HUST. All mice were given free access to food and water. After acclimatized to the environment for two weeks, mice were randomly assigned into five groups as follows: normal diet (ND), high fat diet (HFD), HFD + rAAV-TBG-GFP, HFD + rAAV-TBG-miR-320-3p, and HFD + rAAV-TBG-anti-miR-320-3p, which were injected with corresponding rAAVs (1×10^{10} virion particles in 100 μ L sterile PBS) via tail vein, respectively, as described above. Control mice were injected with an equal volume of PBS. Two weeks post rAAV injection, dietary intervention with an HFD (60% calories from fat, Cat# D12492, HFK Bioscience, Beijing, China) or a ND (11.4% calories from fat, Cat# D12450B, HFK Bioscience, Beijing, China) were conducted for 4 weeks. During the dietary intervention, blood Lipid concentrations of mice were determined every week. At the time of sacrifice, mice were anaesthetized by the mixture of xylazine and ketamine and blood were collected via postcava puncture into EDTA-containing tubes. After sacrificing the mice by an overdose of anaesthesia with 1% pentobarbital sodium (100 mg/kg, i.p.), tissues were taken and immediately frozen in liquid nitrogen.

Histological and cellular analysis

Fresh specimen of mice liver tissues were embedded in paraffin after fixation with 4% paraformaldehyde (pH 7.4) and dehydration, or embedded in OCT follow by frozen in liquid nitrogen. Tissues in paraffin was sectioned at 5 μ m and subjected to standard haematoxylin and eosin (HE) staining. Frozen tissues were sectioned at 10 μ m, fixed with paraformaldehyde and stained by Oil Red O (ORO).

To visualize lipid accumulation in cultured L02 cells, cell monolayers in 24-well plate were subjected to BODIBY 493/503 fluorescent dye (Thermo Fisher Scientific, Waltham, MA) staining according to the manufacturer's instructions. To determine the LDL uptake of L02 cells with different treatment, LDL from human plasma complexed with pHrodo Red dye (pHrodo Red-LDL, Thermo Fisher Scientific, Waltham, MA) was used according to the manufacturer's instructions.

Images of tissues and cells were observed and photographed by an Olympus microscope (Tokyo, Japan) for further analysis.

Determination for lipid concentrations

Lipids were extracted from liver tissues of mice using the mixture of chloroform and

methanol (ratio 2:1). For the extraction of lipid from cultured L02 cells, the cells with different treatment were scraped in PBS and disrupted by ultrasonication. Triacylglycerol concentrations in the liver tissues and L02 cells were measured with the Triglyceride Quantification Assay Kit (Jiancheng Biotech, Nanjing, China) according to the manufacturer's instructions, respectively. Cellular protein content was determined by the Bradford method for well-based normalization purposes. Values of liver tissues were calculated as mmol / (g wet weight).

The concentrations of TG in the medium of L02 cells and plasma TG, TC, and LDL-C of mice were determined with corresponding commercial kits according to the manufacturer's instructions (Jiancheng Biotech, Nanjing, China).

Fast protein liquid chromatography (FPLC) analysis

An equal volume of plasma from each mouse of the same group was pooled. The pooled plasma was separated on a Superose 6 10/300 GL column (GE Healthcare, Boston, MA) at a flow rate of 0.5 ml/min. From 20 to 60 min post-injection, fractions were collected at one-minute intervals. TG and TC levels of these fractions were determined using commercial kits according to the manufacturer's instructions.

mRNA or microRNA sequencing

Total RNA was isolated from Mut and WT L02 cells with TRIzol. mRNA or microRNA sequencing assays and analysis were conducted by personalbio (Shanghai, China).

Bioinformatic analysis

We obtained uniformly processed, consolidated epigenome data of histone markers ChIP-seq and DNase-seq from the ENCODE consortium for human liver tissue (biosample: ENCBS631TVY; assay for H3K4me1: ENCSR642HII; H3K27ac: ENCSR678LND; H3Ka7me3: ENCSR904LIL) and HepG2 cell lines (biosample: ENCBS270KOG and ENCBS645YGY; assay for H3K4me1: ENCSR000APV; H3K27ac: ENCSR000AMO; H3Ka7me3: ENCSR000DUE). GWAS-identified SNPs were collected in the NHGRI-EBI GWAS Catalog, published jointly by the National Human Genome Research Institute (NHGRI) and the European Bioinformatics Institute (EMBL-EBI). Restriction enzyme recognition sites were from REBASE. Bioinformatic analyses on candidate causal SNPs were performed using publically available data from HaploReg Tool. This software includes data on linkage disequilibrium (LD), chromatin state, protein binding annotation, sequence conservation across mammals, and SNP effects on regulatory motifs. Position Weight Matrices (PWMs) were obtained from a published library(Kheradpour and Kellis, 2014) collected from TRANSFAC, JASPAR, protein-binding microarray experiments and ENCODE ChIP-seq experiments. Published data(Thurman et al., 2012) were accessed to identify locations of distal, non-promoter DNase I hypersensitive sites (DHS) within ± 500 kb of MIR320A promoter DHS at threshold = 0.7. Bioinformatics websites miRBase, TargetScan, PicTar, DIANA, and RNAhybrid were used for predicting miR-320a targets.

Statistical analysis

All data are shown as means \pm SEM unless otherwise noted. The Shapiro-Wilk test was used for assessing normality. The Mann-Whitney U test was used for nonparametric data, whereas normally distributed data were compared with Student's unpaired t tests or one-way ANOVA with post-hoc Bonferroni's correction. Significance was set at $P < 0.05$. All statistical analyses were performed in GraphPad Prism version 6.0 (GraphPad Software, San Diego, CA) and SPSS for Windows version 22.0 (IBM Software, armonk, NY) unless otherwise stated.

Supplemental References (Related to Transparent Methods)

- Cui, G., Li, Z., Li, R., Huang, J., Wang, H., Zhang, L., Ding, H., and Wang, D.W. (2014). A functional variant in APOA5/A4/C3/A1 gene cluster contributes to elevated triglycerides and severity of CAD by interfering with microRNA 3201 binding efficiency. *J Am Coll Cardiol* **64**, 267-277.
- Jellinger, P.S., Smith, D.A., Mehta, A.E., Ganda, O., Handelsman, Y., Rodbard, H.W., Shepherd, M.D., Seibel, J.A., Dyslipidemia, A.T.F.f.M.o., and Prevention of, A. (2012). American Association of Clinical Endocrinologists' Guidelines for Management of Dyslipidemia and Prevention of Atherosclerosis. *Endocr Pract* **18 Suppl 1**, 1-78.
- Kheradpour, P., and Kellis, M. (2014). Systematic discovery and characterization of regulatory motifs in ENCODE TF binding experiments. *Nucleic Acids Res* **42**, 2976-2987.
- Kim, Y.B., Komor, A.C., Levy, J.M., Packer, M.S., Zhao, K.T., and Liu, D.R. (2017). Increasing the genome-targeting scope and precision of base editing with engineered Cas9-cytidine deaminase fusions. *Nat Biotechnol* **35**, 371-376.
- Painter, J.N., Kaufmann, S., O'Mara, T.A., Hillman, K.M., Sivakumaran, H., Darabi, H., Cheng, T.H.T., Pearson, J., Kazakoff, S., Waddell, N., et al. (2016). A Common Variant at the 14q32 Endometrial Cancer Risk Locus Activates AKT1 through YY1 Binding. *Am J Hum Genet* **98**, 1159-1169.
- Rendeiro, A.F., Schmidl, C., Strefford, J.C., Walewska, R., Davis, Z., Farlik, M., Oscier, D., and Bock, C. (2016). Chromatin accessibility maps of chronic lymphocytic leukaemia identify subtype-specific epigenome signatures and transcription regulatory networks. *Nat Commun* **7**, 11938.
- Thurman, R.E., Rynes, E., Humbert, R., Vierstra, J., Maurano, M.T., Haugen, E., Sheffield, N.C., Stergachis, A.B., Wang, H., Vernot, B., et al. (2012). The accessible chromatin landscape of the human genome. *Nature* **489**, 75-82.
- Yin, Z., Zhao, Y., Li, H., Yan, M., Zhou, L., Chen, C., and Wang, D.W. (2016). miR-320a mediates doxorubicin-induced cardiotoxicity by targeting VEGF signal pathway. *Aging (Albany NY)* **8**, 192-207.